

THE FLORIDA AGRICULTURAL AND MECHANICAL UNIVERSITY
COLLEGE OF ENGINEERING

SYNTHESIS AND ANALYSIS OF SPHERICAL CVTs FOR VARIABLE
STIFFNESS APPLICATIONS

By

Twan P. Capehart

A Dissertation submitted to the
Mechanical Engineering Department
in partial fulfillment of the
requirements for the degree of
Doctor of Philosophy

Tallahassee, FL

Spring, 2020

The committee approves the dissertation entitled, Synthesis and Analysis of spherical CVTs for Variable Stiffness Applications by Twan Capehart, defended on Wednesday, April 08, 2020.

Dr. Carl A. Moore
Professor Directing Dissertation

Dr. Jonathan E. Clark
Committee Member

Dr. William Oates
Committee Member

Dr. Clement Allen
Outside Committee Member

Approved by:

Name of Department Chair, Degree, Chair, Name of Department

J. Murray Gibson, Ph.D., Dean, FAMU-FSU College of Engineering

David H. Jackson, Jr., Ph.D., Associate Provost for Graduate Education and Dean of Graduate Studies Research

DEDICATION

I would like to dedicate this accomplishment to my entire family, for they are the driving force that drives me to strive for greater things every day. I love you all. I extend a special and most important dedication to my son, Twan P. Capehart Jr. the pride and joy of my life. I love you little one.

ACKNOWLEDGMENT

I would like to acknowledge Dr. Carl Moore as my mentor. I appreciate you taking me under your wing, showing me patience and always believing in me. I appreciate you. Thank you also to Dr. Jonathan Clark for being more than a committee member. Thank you for the extra attention, support and motivation. Thank you to my committee members for your service.

Thank you to my friends and family for great support. Thank you to my lab mates for being the best team of support, knowledge and inspiration a graduate student can have.

CURRICULUM VITAE

Academic Objective:

Ph. D. Candidate, Mechanical Engineering (Variable Stiffness Robotic Applications – Florida A & M University)

Education:

Masters of Science-Mechanical Engineering, Florida A&M University, April 27, 2012, *GPA 3.53*

Bachelors of Science (Cum Laude)-Mechanical Engineering, Florida A&M University, April 30, 2010, *GPA 3.17*

Papers/Presentations:

October 13-15, 2018

Design and Analysis of a Novel Variable Stiffness Joint for Robot
2018 5th International Conference on Mechanical, Materials and Manufacturing, Orlando, Florida

-Authors: Xiang Zhang, Twan Capehart, Dr. Carl Moore

March 13-14, 2016

Competitor in 3Minute These Competition at FAMU
Bio-Inspired Robotics - Realizing Variable Stiffness Mechanics

November 18, 2015

Variable Stiffness Mechanisms Using Spherical Continuously Variable Transmissions

International Mechanical Engineering Congress and Expo, Houston, Texas

-Authors: Capehart, Twan; Moore, Dr. Carl A.

May 16, 2013

Design of a Continuously Variable Amplification Device

Florida Conference on Recent Advances in Robotics and Robot Showcase

-Authors: Little, Kirby; Roberts, Dr. Rodney; Moore, Dr. Carl A.; Capehart, Twan; Walsh, Dr. Kenneth

September 13, 2012

Variable Impedance CVT Mechanisms for Electromechanical Systems
Student Research Forum , Florida A & M University

-Presented research poster to faculty and industry members on variable impedance devices and current research progress.

-Second Place – Graduate students in engineering and environmental sciences.

Professional

Development Activities

September 26-29, 2017

Selected to attending NEXTPROF Fall 2017 at University of Michigan Engineering Dept.

June 13-17, 2016

Instructor for High School Robotics Camp Under Dr. Shonda Bernadin

Spring 2016

Student Representative, Engineering Dean Search Committee

Spring 2016, Spring 15, Fall 2014, Spring 2013	<i>Teaching Assistant for Mechanical Systems I &II, Dynamic Systems I, Advanced Dynamics</i>
November 18, 2015	<i>Technical Presentation at IMECE 2015, Houston, Texas</i>
June 2013,2014,2015	<i>President/ Instructor of AEIMD Summer Science Camp</i>
February 7-8, 2013	<i>Accenture Case Competition, FAMU, Tallahassee, Florida (1st Place)</i>
September 13, 2012	<i>Student Research Forum, FAMU, Tallahassee, Florida (2nd Place in Category)</i>
November 18-19, 2011	<i>QEM Network Workshop For Engineering Faculty on the Professional Development and Mentoring of Underrepresented Minority Graduate Engineering Students, Baltimore, Maryland</i>

Affiliations:

Graduate Student Advisory Board (FAMU-FSU College of Engineering)

- 2013-2016 Chair – Leader of advisory board. Directed meeting structure, topics and cultivated environment for progressive brainstorming. Structured Annual Recommendations report. Liaison between GASB and college administration.

National Society of Black Engineers (NSBE):

- 2010-2011 Chapter President - Leader of Chapter Executive Board and membership. Point of Contact of corporate affiliations and chapter business. Provide vision and direction for chapter membership.
- 2009-2010 Region 3 Academic Excellence Chairperson- Regional Chair for all business involving Academic Excellence initiatives and programs in Region 3 (6 States, 67 Chapters)
- 2008-2009 Chapter Conference Planning Chair- In charge of all aspects of planning and organization for Conferences that the FAMU-FSU Chapter participates in.

Society of Automotive Engineers (SAE):

- 2008-2010 FAMU Treasurer- In charge of organization of finances in two club accounts.

Technical Training:

SolidWorks; Pro-Engineer; Adams; LabVIEW; Working Model; MATLAB; Simulink; Latex; VisualBasic; Java; C-Programming ; MathCad, Arduino

Table of Contents

ABSTRACT	xi
LIST OF FIGURES	xiii
LIST OF TABLES	xvi
CHAPTER 1: INTRODUCTION	1
1.1 Motivation	1
1.2 Problem Statement	3
1.3 Contributions	4
1.4 Dissertation Outline	5
CHAPTER 2: BACKGROUND	7
2.1 Compliance Systems in Robotics	7
2.2 Compliance in Legged Locomotion	9
CHAPTER 3: SIMULATIONS OF SPHERICAL CVTS FOR ROBOTIC APPLICATIONS	12
3.1 Introduction	12
3.2 The Spherical CVT	13
3.3 CVT Scaling Simulations	16
3.3.1 Model Validation	17
3.3.2 Box Vs. Tetrahedral Configuration	21
3.4 Variable Stiffness CVT Concept	22
3.4.1 Theoretical Variable Stiffness CVT	23
3.5 Variable Stiffness CVT Application	25
3.6 Simulation Results	26
CHAPTER 4: ROBOTIC SCALE CVT DESIGN	29

4.1 Geometric Scaling.....	29
4.2 Alignment by Part Reduction.....	30
4.3 The CVT Contact Patch.....	32
4.4 Material Selection and Customized Components.....	34
4.4.1 CVT Custom Support.....	34
4.4.2 Transmission Sphere.....	35
4.4.3 Drive Rollers Selection.....	37
4.4.4 Steering Rollers.....	39
4.4.5 Preloading Platform.....	41
4.5 Design Conclusions.....	43
CHAPTER 5: VARIABLE STIFFNESS CVT.....	45
5.1 Introduction.....	45
5.2 VSCVT Prototype.....	46
5.3 VSCVT Application.....	49
5.4 Experimental Validation of Variable Stiffness.....	53
5.4.1 Impact Pendulum Test.....	53
5.4.2 Impact Test Results.....	55
5.4.3 The Variably Compliant 1-Legged Hopper.....	56
5.4.4 Disturbance Rejection on Various Substrates.....	58
5.4.5 Hop Amplitude Matching on Different Surfaces.....	62
5.5 Experimental Conclusion.....	65
CHAPTER 6: CONCLUSION.....	66
REFERENCES.....	69
APPENDICES.....	74

Appendix A: VSCVT Assembly Process: 74
Appendix B: CAD Drawings of CVT Custom Support..... 75
Appendix C: Teensy 3.2 Control and Data Acquisition Program 80

ABSTRACT

Robust and efficient robotic locomotion is critical if robots are to leave the laboratory and operate successfully in unknown and unstructured environments. While computer vision and control are important components of robot navigation, many researchers, inspired by biological systems, have focused on improving the mechanical ability of robots to navigate unstructured terrain. For these researchers, the development of competent legs is believed to be indispensable to successful mobility in much of our natural world.

As opposed to stationary robots, those robots with mobile platforms have nearly unbounded workspaces. Their freedom of movement makes them obvious candidates for a large set of applications including search and rescue, surveillance, human assistance and rehabilitation. While wheeled and track driven platforms are in abundance and perform quite well, biological inspiration beckons us to develop more leg driven platforms. The use of legs offers an increased functionality and dexterity that is not available with wheels or tracks. More importantly, in field robotics and other non-structured settings, robots with compliant legs are more capable of traversing uneven and unknown environments that contain larger perturbations. With this understanding, the research focus of this thesis is on a growing subset of legged robotics - compliant robotic limbs.

Compliance is readily becoming an ally in robotics because of the recent ability of scientist and engineers to understand and leverage its benefits in computation and design [1]. Alexander explains that the elastic elements in animals of all sizes do a significant amount of work during locomotion for stability and energy savings [2]. According to biological researcher Andrews, animals use passive and active elastic elements to maneuver efficiently and to achieve higher locomotion speeds [3].

In this research, we will present a mechanical device to provide variable compliance. This novel device, named the Variable Stiffness Continuously Variable Transmission (VSCVT), is intended to give a robotic limb the ability to change its effective stiffness rapidly in real-time [5]. Rapid compliance change is a proven capability of animals which enables them to handle real-time locomotion uncertainties and other changes in their environment [4]. We will present the details of the VSCVT design and simulated operation as well as experimental results that validate its ability to improve robot legged locomotion.

LIST OF FIGURES

Figure 1: Diagram of the SLIP model template during a single step cycle. A system is reduced to a point mass, with a massless leg with stiffness (k) and length (L).....	10
Figure 2: Spherical CVT and its working components.....	14
Figure 3: Diagram of Box CVT and its working components.....	15
Figure 4: Adams model of a spherical CVT for simulated scaling.....	16
Figure 5: Simulated speed ratio of scaled down CVT	18
Figure 6: CVT velocity negligible to CVT operation performance.....	19
Figure 7: Proportional relationship between sideslip and Perpendicular torque	21
Figure 8: Tetrahedral vs Box Configuration with respect to sideslip.....	22
Figure 9: Diagram of Series Elastic actuator	22
Figure 10: Diagram of the series variable stiffness CVT	23
Figure 11: Variable stiffness simulation of VSCVT showing change in displacement by varying transmission angle	27
Figure 12: Variable stiffness values using a CVT at various transmission ratio. a 4x increase in stiffness is achieved over the transmission operation range.....	28
Figure 13: Size comparison of current CVTs to small-scale CVT for Variable Stiffness	30
Figure 14: Reduction in number of parts to house the working parts of the CVT	31
Figure 15: Visual representation of the deformation of materials in rolling contact under some preload force.....	32

Figure 16: Wear on roller shafts as a result of the shear forces in the contact patch.....	33
Figure 17: Left is an aluminum CVT support, and at right is a 3D printed ABS CVT support, both have bearings inserted into the provided housings.	35
Figure 18: Diagram of forces of interest acting on the transmission sphere in a spherical CVT.....	36
Figure 19: Multiple Materials of Spheres and Drive Rollers for Comparison as CVT working components.....	37
Figure 20: Diagram of forces of interest acting on the drive rollers in a spherical CVT .	38
Figure 21: Custom steering roller shafts assembly. The steering roller, steering roller shafts and preloading Belleville springs are pictured here.	40
Figure 22: CVT preload mechanism used to assembly the CVT and apply preload.....	42
Figure 23: Physical prototype of the small CVT. In the picture to the right the CVT is attached to its elastic element, making the Variable Stiffness CVT.....	47
Figure 24: Conceptual diagram of variable stiffness hopping application	50
Figure 25: Adams simulation of a variable stiffness 1D hopper performing multiple robotic tasks	51
Figure 26: The impact pendulum experimental platform used to test VSCVT response to impact forces of hopping	54
Figure 27: Experimental results of VSCVT response to Impact force using different transmission angles	56

Figure 28: 1-Legged hopper experimental platform used to analyze VS-Hopper. Notice the rack and pinion coupling of the VSCVT and the robot leg in the top-right photo and the elastic element in the bottom right photo..... 57

Figure 29: Conceptual representation of Decay Ratio analyzed over a step perturbation 60

Figure 30: Experimental results of Disturbance rejection testing of VS-Hopper for recovery on Polyethylene Foam surface. Validation of VSCVT as an effective variable stiffness device and shows improved stability by adding the VSCVT..... 61

Figure 31: Hopping Amplitude of the 1D hopper on multiple surfaces. It is show on multiple data sets that hop amplitude can be matched on different surfaces using CVT control. 63

Figure 32: Visualization of hop amplitude matching when transition surfaces by controlling the VSCVT transmission ratio 64

LIST OF TABLES

Table 1: CVT Mechanical Properties used in the ADAMS simulation and in published experiments.	17
Table 2: 1 legged hopper with variable stiffness CVT Simulation Parameters	26
Table 3: List of the selected components for the VSCVT physical prototype	43

CHAPTER 1

INTRODUCTION

1.1 Motivation

Humans throughout history have tried to create machines that mimic the appearance, mobility, functionality, intelligent operation, and thinking process of biological creatures [2]. Similarly, the computer industry has expended effort to develop computers with capabilities closer to that of the human brain. In conjunction, engineers have intensified their focus on the electromechanical systems controlled by these powerful computers. Robotics researchers are also fascinated with how well natural systems adapt and thrive in highly unstructured environments. Their fascination drives research to develop robots that can adapt and thrive in the real world. In this thesis, we will focus on the realm of robots whose functionality, design and/or aesthetics are motivated by biological systems. This research topic has been appropriately coined bio-inspired robotics.

Bio-inspired robotics is a merger of the biomechanical studies of biological systems and engineers drawing principals from this inspiration to drive the development of a robot system. One may ask the general question of what it means to be biologically inspired. Many different degrees of inspiration are possible, from vague resemblance to strict emulation. Consider robot locomotion. For the simplest biological inspiration, we may build robots that use legs because they more resemble animals which use legs rather than wheels. At the other extreme, we could literally try to emulate, in every detail, the type of legs and the particular crawling gait of a species of insect [1, 6].

Consider human inspired robotics. There are industrial grippers which incorporate flexible

joints and soft surfaces to mimic human hands but with increased gripping ability [7]. Robotic manipulators like the Schunk 7DoF have been designed to traverse larger workspaces using hand-like grippers to handle objectives that previously required a human [Schunk]. These and other robotic systems were inspired by the functionality of the human hand/arm combination.

Within the arena of field robots, locomotion is a critical part of expanding the way robots can interact with the greater environment. Whether land, air or sea, the ability to traverse large areas compared to a robot's functional workspace exponentially increases its available applications. When thinking of land based mobile robots, we readily think of wheeled or track driven robots. Wheels and tracks both have their advantages and disadvantages, but they are interchangeable for most tasks. Robotics platforms with wheels can travel over large areas while maintaining stability relatively easily over roads and flatter terrains. As terrains become rough and difficult to traverse, track driven robots with their higher torque and improved traction are the traditionally preferred mode of locomotion. But still, the overwhelming majority of outdoor terrains are quite irregular and cluttered.

As terrain becomes less consistent, rougher, changes elevation and become cluttered with obstacles, wheel and tracked modes of locomotion are less viable. For instance, when a search and rescue mission is needed after an earthquake, wheeled vehicles are less reliable because of the unstructured environment. Humans and animals use their legs to make this and similar task possible without much effort. Studies into legged robotics are necessary to unlock applications where locomotion in highly perturbed environments is a requirement to successfully reach difficult locations. Sayyad states a good summary of the motivation behind modern robot locomotion research, "The reason behind such sustained interest in legged robots is due to the

fact that most of the earth's land surface is inaccessible to wheeled or tracked systems. Legged animals can, however, be found everywhere.”

Legged robots have developed rapidly through engineering research, mainly because of our ability to study a large variety of legged creatures. From crickets and roaches, to horses and humans the mechanics of biological systems and their locomotion characteristics have received a large amount of attention from the engineering community, and a major focus has been on the capabilities of legs. The seven-link biped [8] and Rabbit are examples of robots that can successfully perform the complex task of walking. Asimo [9] and Wabian [10] take it one step further and combine robotic arms, legs and torso to produce humanoids that are very capable of stable walking, a very good form of locomotion. These robots have the look or functionality of biological systems, but they are not fast, nor are they energy efficient or robust to uncertainties in their work environment. The inspiration from biology that produces these types of robots capture functionalities very well but is lacking the use of the more vital elastic elements embedding in humans and animals. Raibert successfully exploited compliance in his first 1 legged hopper using air springs to produce very impressive dynamic behaviors [11]. Over the last few decades, engineers have been incorporating compliance into robots wherever possible and have understood that without it efficient, fast and stable locomotion is extremely difficult and complex.

1.2 Problem Statement

The addition of compliance has added another necessary dimension to the improvement of robotic systems. The next step being taken by the community is to give these robotic mechanisms a way to adjust their compliance to adapt to their environment or tasks, similarly

to biological systems.

In this research we present a novel variable stiffness mechanism. The mechanism, known as the variable stiffness spherical continuously variable transmission (VSCVT), can be used to create a variably compliant elastic element by controlling the transmission ratio between the input and output rollers of the transmission. This mechanism could address multiple issues in variable stiffness robotics, including low weight and size for legged field applications, fast stiffness adjustment (order of milliseconds), and simple operation principles. Although the device requires a separate actuator to adjust the stiffness, the actuator torque requirements are quite low, allow for use of smaller, less powerful motors. We intend to show that with a proper design focus, a VSCVT can handle the loads required to be effective in a legged hopping application. The effectiveness of the VSCVT is displayed in both simulation and in experiments on a physical platform, where it gives the hopper the ability to adjust its hop height through a change in leg stiffness. Another beneficial effect of the VSCVT is that it affords the hopper the ability to accommodate for varying surface stiffness in-situ with very fast stiffness adjustment.

1.3 Contributions

The overall goal of this dissertation is to the synthesis and analysis of a variable stiffness mechanism applied to robotic applications using a millimeter scale spherical continuously variable transmission. In order to be a useful mechanism in legged robotics the scale of a spherical CVT must be on par with the scale of the intended robotic systems. Typically, these legged systems average a maximum length of about one meter and a mass limit of twenty kilograms. These are considered to be carryable robots for a 1-man team. A spherical CVT of

about two percent of the size of current CVTs used in previously published technical papers is needed to actually be applicable to legged locomotion. Simulations of the spherical CVT on a millimeter scale show that the performance metrics trends are consistent with larger scale CVT's. These results also uncover the operational limits of the CVT at this scale, aiding in the identification of the range of applications for the mechanism.

A drastic reduction in scale requires specific design considerations to realize a functional prototype. Size and weight requirements were established based on the eventual application. Components were selected based on size constraints, assembly considerations, reliability and operational performance. Custom components were designed, assembled and finally coupled to an elastic element to create a novel VSCVT. The prototype was tested in experimental applications. An impact pendulum was used to test the VSCVT response to impact forces. Then with the VSCVT attached to a 1-legged robotic hopper (VS-Hopper) its effectiveness as a variable stiffness device was demonstrated by its ability to effect hop height. Finally, the VS-hopper performance was analyzed on multiple surface and shows that the legged robot equipped with a VSCVT is variably stiff. The hopper can adjust hop height with changes in CVT steering angle, and more impressively the hopper can maintain hopping performance across multiple surfaces by adjusting the steering angle.

1.4 Dissertation Outline

This dissertation presents the VSCVT from conceptual development to physical robot platform analysis as follows: Chapter 2 is a presentation of relevant background research on the multiple engineering aspects including robotic locomotion with a focus on legged

robots, continuously variable transmissions use in robotics, the design considerations for relevant CVTs and the use of compliance in robot extremities.

Chapter 3 is a roadmap of the development of the concept of a variable stiffness CVT. The relevant CVT performance parameters are evaluated for miniaturizing a known CVT design using computer simulation and compared to results presented in literature. The concept of a VSCVT for robotic applications is described in detail. The VSCVT design is discussed in theory, and the device is tested in ADAMS simulation package.

Chapter 4 is an in-depth description of the synthesis process of the VSCVT and its working components. The design parameters of the CVT mechanical support structure at the required scale and material selection process for the contact components are considered and analyzed. Five different materials are physically tested and compared for their viability in the final design. The contact patch mechanics are also explored for insight on the expected performance of the selected materials.

Chapter 5 presents the physical prototype of the VSCVT and its application as a variable stiffness robotic mechanism. The VSCVT installation is briefly described, with an emphasis on the coupling to the robotic leg. Impact test results are presented in relation to the physical bandwidth of the CVT using a pendulum test. The hopper is experimentally analyzed for both transient behavior due to large perturbations and stability analysis during terrain transition.

Chapter 6 concludes with a summary of the previous chapters and a focus on future works.

CHAPTER 2

BACKGROUND

Variable Stiffness research is an emerging area in the robotics research community. Researchers who focus on structures, materials, sensors, control, and mechanical design are contributing to variable stiffness systems to create robots with a higher level of adaptability and improved performance. Similarly, Human-Robot interaction (HRI) researchers have found that creating variable stiffness robot links can make robots safer in the presence of human. Larger scale applications such as structure and building designs are also looking into variable stiffness devices to improve the structural integrity in face of earthquakes and hurricanes. Finally, bio-inspired robotics researchers have taken notice that the variable stiffness capabilities exhibited in animals is the key to many of the dynamic movements they can perform.

2.1 Compliance Systems in Robotics

Biologists have long known that mechanical stiffness and compliance in animals is indispensable for navigating their environments. Research as early as 1964 by Cavagna determined that springs are a vital component in energy-savings for humans and animals [12]. Biological studies like that by Biewener et. al [6] on horse running, determined that elastic tendons produce up to forty percent of the positive work necessary during trotting. Similarly, Alexander found that animals store energy in elastic muscles to generate power for dynamic movements [2]. Engineers are also investigating compliance in many forms, including variable stiffness, to improve robotic systems. As stated by Miller et al., mechanisms for stiffness adaptation range from mechanical solutions to smart material

approaches [4]. In this thesis I focus on the mechanical approaches to variable stiffness. One example is Raibert use of springs in his hopper to create a human inspired leg that can balance and hop [11]. Later, Pratt published *Stiffness Isn't Everything* explaining the need for less stiff actuator-load interfaces in robots and for safer interaction between robots and the surrounding environment [1].

More recently, several researchers have studied methods to achieve variable stiffness. Systems like the robotic joints and limbs developed in the DLR Hand Arm System presented by Grebenstein et al. [7] are capable of adjusting their impedance using complex electronic control and mechanical design. Mechanisms that are less computationally expensive have also been able to achieve some form of variable stiffness. The review of variable stiffness mechanism presented by Ham [13] is a good representation of how elastic elements are used in these mechanisms. Likewise, Hurst et al. demonstrates how springs can be used in an antagonistic manner, as in animal muscles, for his actuator design [14]. There are also many systems in which the stiffness variability is achieved through a flexible structure. For example, Galloway et al. uses tunable C-legs [15] whose stiffness can vary through lever arm adjustment when the robot is stationary. The VS-joint stiffness used in the DLR Hand Arm System is also varied mechanically [7]. Through a custom designed cam and spring combination, the stiffness of the fingers' joints and positions can be changed independently using motors.

Enoch states in a research document on a bipedal robot named BLUE that variable stiffness designs can be broken down into three major categories: antagonistic, series pretension, and tunable springs which are described below based on Enoch's research [16].

Antagonistic designs typically have two actuators pulling through springs series, and alter stiffness by co-contracting these springs. Non-linear springs are required for most antagonistic designs so most variable stiffness research on these devices focus on creating a suitable non-linear spring [17] [18] or arranging linear springs in such a way as to create non-linearity [19]. A significant amount of energy is usually needed to vary the stiffness.

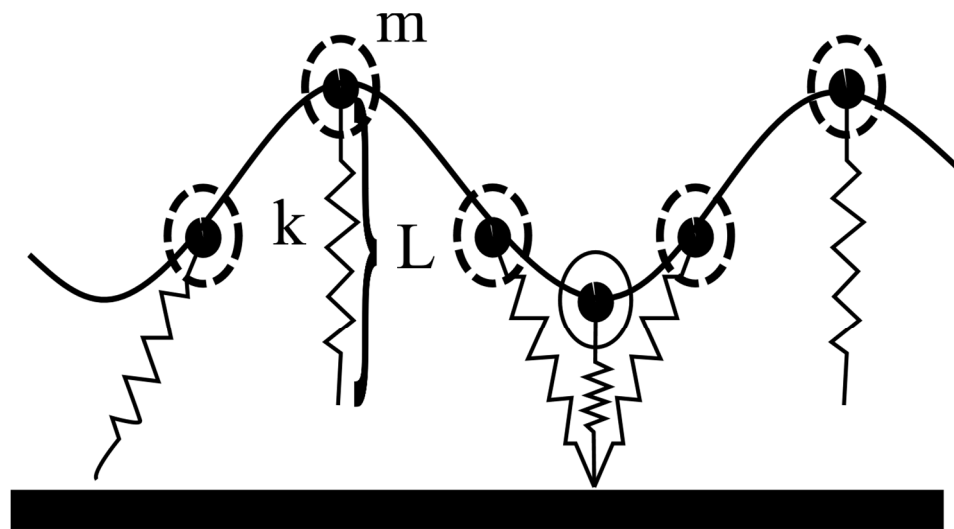
Series pretension devices have a spring in series with the actuator so that the spring can be pre-stressed in order to increase joint stiffness [20] [21]. This type of pretension device also requires energy to change stiffness.

Tunable spring designs rely on changing the geometry of a compliant element in series with an actuator in order to adjust the stiffness [22] [23] [24]. The tunable stiffness devices usually have a smaller compliance, but the required energy to change stiffness is also low. The variable stiffness device proposed in this research is a tunable stiffness device, which uses the geometric relationship of the components in a friction drive transmission to modulate the system stiffness.

2.2 Compliance in Legged Locomotion

Legged locomotion is a process involving a coupling of complex system kinematics and dynamics but is performed seamlessly by biological systems. Common to the scientific method, the hypotheses, analysis, and final replication of these systems is accomplished by developing simplified representations that reduce complexity but maintain some level of similarity to the original system. For legged locomotion Full and Koditschek deemed these simplified models “templates”, stating that a template is the simplest model (least number of variables and parameters) that exhibits a targeted behavior [25]. The Spring-Loaded

Inverted Pendulum (SLIP) model is a proven template for legged locomotion that is used to design single and multi-legged robotic systems for simulated and experimental research. A schematic of the SLIP model template is shown in Figure 1. In the most basic form the SLIP model uses the mass (m), stiffness (k) and leg length (L) of a system to map out locomotion characteristics and force profiles generated for walking, running, hopping and other locomotion modes.



Simplified 2D SLIP Model

Figure 1: Diagram of the SLIP model template during a single step cycle. A system is reduced to a point mass, with a massless leg with stiffness (k) and length (L).

Multiple variations of this template have been developed to study control schemes in legged locomotion and construct experimental robotic platforms [26] [27] [28] [29]. The adaptability of the template has enabled researchers to vary the model's parameters

including stiffness and leg length and to add damping and actuation [30]. Studies show that the adjustment of one or more of these parameters is necessary for robots to adapt to changes in their environment and to maintain performance standards [4]. In this dissertation a 1-D version of the SLIP model template is used to test the impact of leg stiffness variation in both simulation and experimentation.

CHAPTER 3

SIMULATIONS OF SPHERICAL CVTS FOR ROBOTIC APPLICATIONS

3.1 Introduction

The foundation of my tunable spring variable stiffness device is a continuously variable transmission or CVT. CVTs of many variations and sizes have been used for centuries in many applications as varied as automobiles, drill presses mechanical computation and bicycles. In 1490 Leonardo da Vinci conceptualized a stepless CVT, and the first patent for a friction based CVT was awarded in 1886 [31]. For over 500 years the CVT concept has progressed into multiple fields with many variations in its design and, over the last few decades, engineers have been incorporating CVTs into intelligent machine designs.

Peshkin and Colgate, in 1999 introduced spherical CVTs in Cobots and showed how they can be used to create haptic devices that impose virtual constraints [32]. Their research proved that CVTs are capable of carrying loads and rapidly changing the gear ratio of a motor during operation. In 2002, Kim et al used the nonholonomic CVT as the drive unit of a wheeled mobile robot [33]. It was concluded that the operational efficiency of the wheel motors can be improved using the CVT as a gearing mechanism to meet operational speed or torque requirements. Finally, Tadakuma et al designed a load-sensitive CVT mechanism in 2011 to automatically adjust CVT transmission angle to produce the torque required to move a linear plate [34]. In the face of a load, the contact angle between the CVT and the linear plate changes proportionally via a mechanical transmission coupled to a non-linear spring, modulating the transmission ratio of the CVT.

The tunable spring based variable stiffness mechanism presented in this thesis uses a spherical CVT coupled with an elastic element to mechanically modulate the device's effective stiffness. The addition of a modular variable stiffness mechanism to a bio-inspired robotic limb can enable the robot to adapt to a multitude of real-world applications. CVTs have been used in many applications, but their coupling to elastic elements for robotic tasks has to my knowledge not been investigated.

This section served as a brief introduction to the history of CVT's. In section 2 of this paper we present and validate a model of a spherical CVT and explain why we chose a non-traditional CVT design. Section 3 introduces our CVT equipped variable stiffness device. In Section 4 we use our device to model a bio-inspired variable stiffness leg concept and perform simulations. In Section 5 we conclude and offer areas for future study.

3.2 The Spherical CVT

The spherical CVT in Figure 2 is a dry-friction transmission where a sphere is caged by multiple rollers and angular momentum is transmitted via the friction forces between the rotating bodies. In a typical design, 4 rollers are arranged about the sphere in a stretched tetrahedral configuration. Two of the rollers are drive rollers (here labeled drive roller 1 and drive roller 2 but sometimes referred to as the input and output rollers) and two are steering rollers, one of which is not shown.

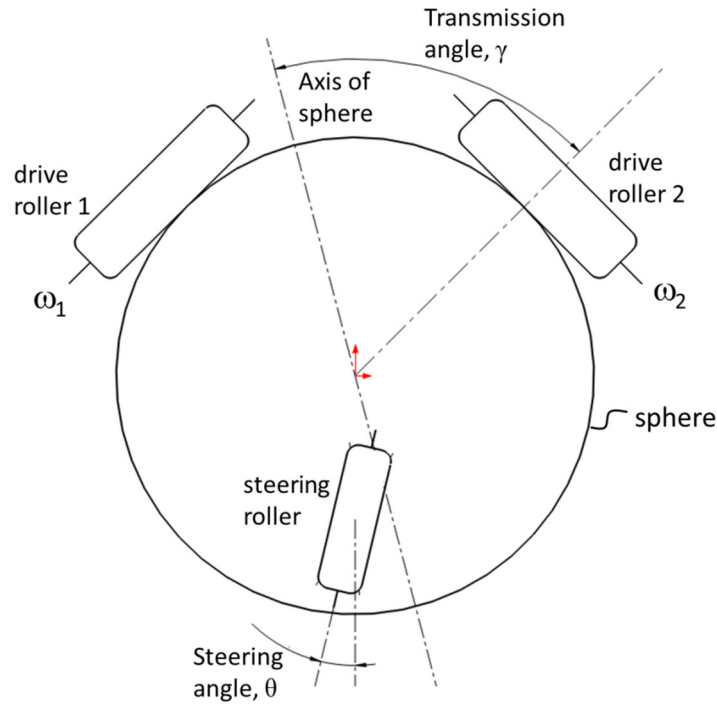


Figure 2: Spherical CVT and its working components

In practice, the drive rollers angular velocities are coupled to the joints of a robot or machine that are to be controlled to a desired speed ratio. Rolling constraints between the rollers and sphere result in the spheres rotational axis lying in the plane of the drive roller. The orientation of the rotational axis (γ) is a function of the steering rollers orientation (θ) such that the drive rollers angular velocity ratio is,

$$T = \frac{\omega_2}{\omega_1} = \tan(\gamma)$$

The tetrahedral arrangement of the rollers is a mechanically attractive design for a CVT because it uses the minimum number of rollers necessary to constrain its sphere. There is also a less popular arrangement called the box CVT shown in Figure 3 which nevertheless has some attractive possibilities. First introduced for cobots consideration by Peshkin and

Colgate [32], the box has six rollers positioned in the center faces of a cube surrounding a central sphere (a second steering roller is under the sphere and not shown but remains aligned with the steering roller on top).

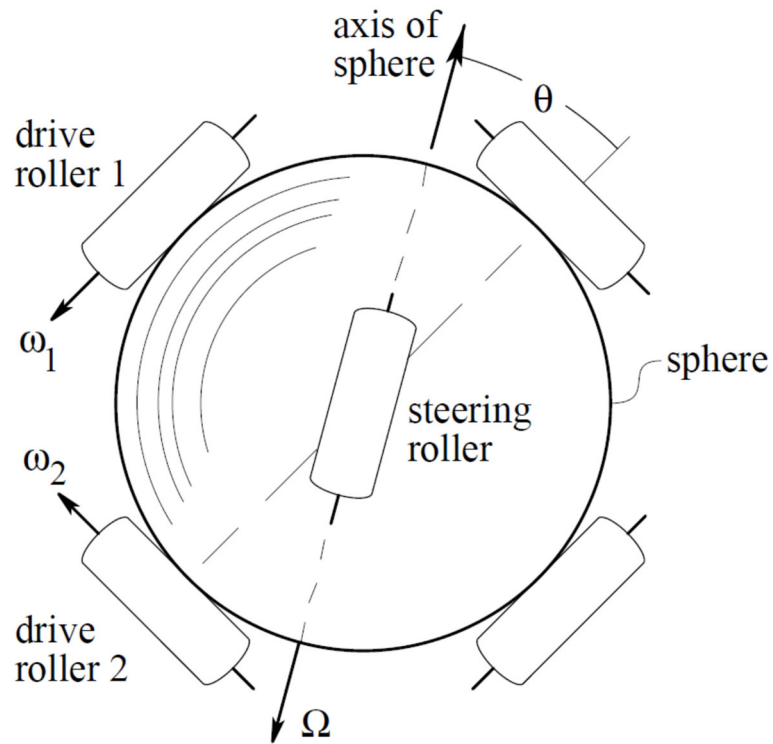


Figure 3: Diagram of Box CVT and its working components

The drawback of this design is the two additional rollers and the requirement that the preload force needed to maintain the rolling constraints must be applied to both the steering and drive rollers independently. Even so, according to research performed by Kim et al. the drive rollers in the box design should experience less slip under resistant torques which reduces the control effort required to maintain desired drive roller speed ratios [35]. An increase in mechanical complexity for a reduction in drive roller slip may be an acceptable tradeoff since our variable stiffness CVT device must have faster reaction times than CVT

equipped cobots. For example, it is not uncommon for a foot of a running robot to be in contact with the ground for only 100 milliseconds per stride [4], leaving little time for controller compensation of roller slip. But before attempting to use simulation to quantify the reduction in slip for the box design we first wanted to verify that our simulator (ADAMS) could successfully reproduce the experimental findings of the more complicated tetrahedral CVT published previously. The most extensive experimentation on the tetrahedral CVT was carried out by Brokowski et al. [36] and Kim et al. [35], so their results are used for our model validation.

3.3 CVT Scaling Simulations

The Adams model of the tetrahedral CVT is shown in Figure 4. Visible are 2 drive rollers on the top, a transmission sphere, and 2 steering rollers on the bottom. The size of the CVT components and some of the more significant mechanical properties of the model and the aforementioned experiments are found in table 1.

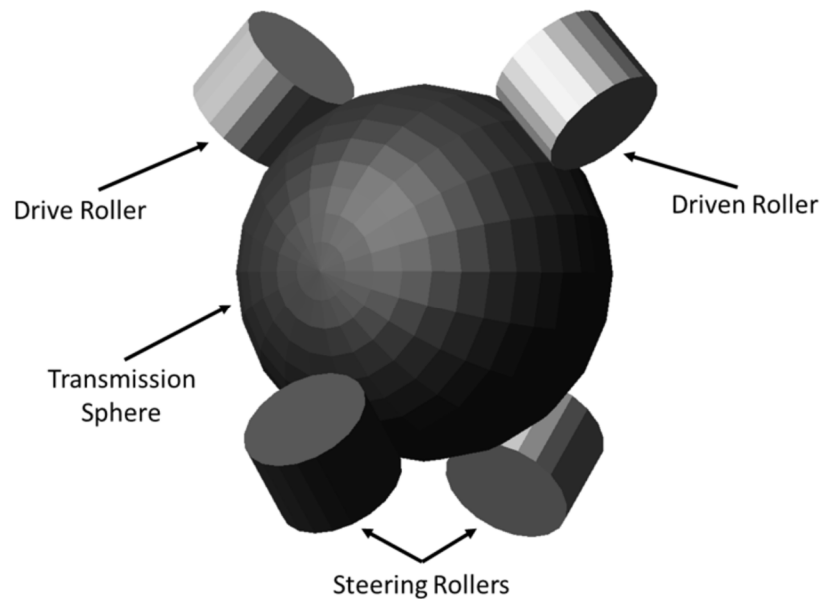


Figure 4: Adams model of a spherical CVT for simulated scaling

3.3.1 Model Validation

To verify our simulated CVT model, we consider three of the most important dynamic responses of a CVT: actual speed ratio as a function of theoretical transmission ratio, roller torque induced slip and slip as a function of drive roller velocity.

Table 1: CVT Mechanical Properties used in the ADAMS simulation and in published experiments.

CVT Parameters	Experimental	Simulation
Sphere Radius	4.25 in	4.25 in
Drive Roller Radius	1.575 in	1.575 in
Steering Roller Radius	1.50 in	1.575 in
Sphere Material	Bowling Ball	Steel
Drive Roller Material	Polyurethane	Steel
Steering Roller Material	Polyurethane	Steel
Preload Force (Equal per roller)	53.2lbs	53lbs
Coefficient of Friction	Unknown	0.7

CVT Speed Ratio

The first comparison is to show that the CVTs velocity relationship between the input and output roller is ideally governed by equation 1. Brokowski has shown, in experimentation, that this ratio follows the trend line governed by tangent (γ) very closely. Deviation from the ideal case is said to be due to the inherent friction loss in a CVT of this configuration, but is usually minimal when no load is applied to the CVT.

To see if the ADAMS simulated CVT is also governed by 1 we commanded an arbitrary speed of 300 rpm on one of the drive rollers. The transmission angle, γ , of the CVT is set

from 10 to 80 degrees, at 10-degree increments, and the speed of the second drive roller is recorded. The speed ratio between these two drive rollers is calculated and graphed in Figure 5 and compared to the ideal speed ratio or $\tan(\gamma)$.

The results in Figure 5 show the same trends as the experimental data; a speed ratio profile very close to the ideal case. It is of note that the CVT operating speed ratio range (-6 to +6) in simulation is similar to the speed ratio range of the experiments; beyond this point the CVT breaks down as the drive rollers experience gross slip.

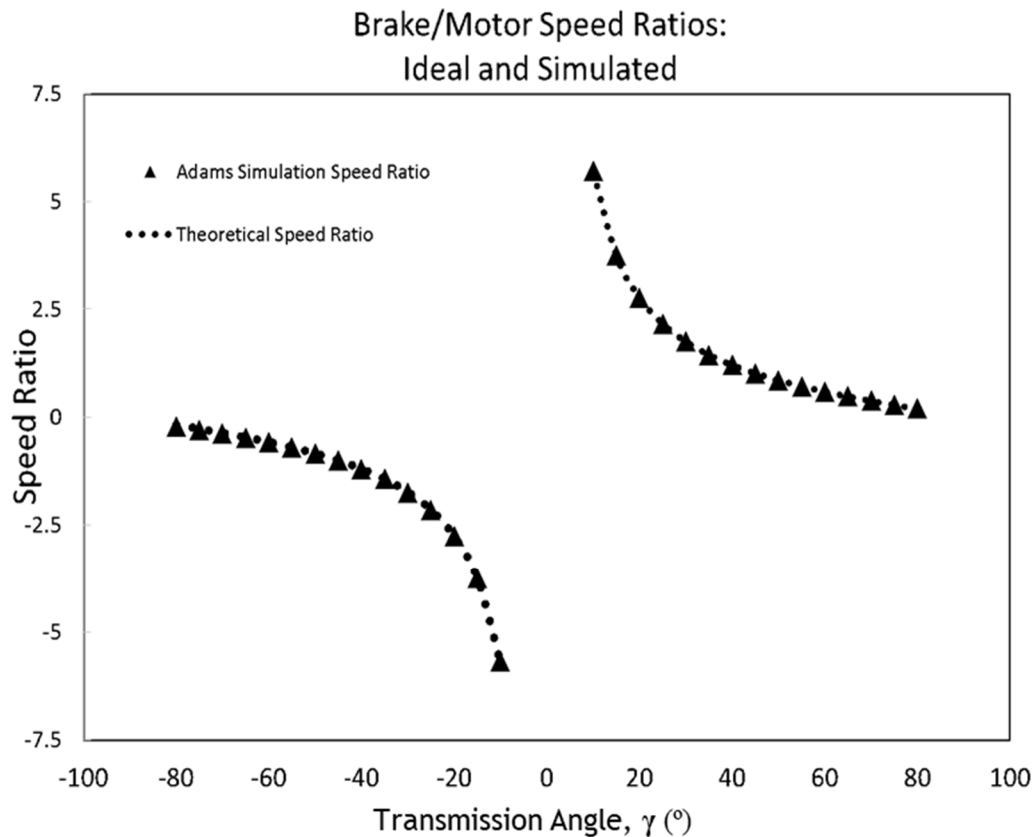


Figure 5: Simulated speed ratio of scaled down CVT

Slip Angle Independent of Velocity

Kim collected data showing that the sideslip angle of a CVT is independent of the CVT input roller velocity. Sideslip angle, also called slip angle (α), is described as the difference

between the desired transmission angle and calculated transmission angle as a result of perpendicular torque on the CVT drive rollers.

$$\text{Slip Angle } (\alpha) = \gamma_{des} - \gamma_{act}$$

Perpendicular torque is a drive rollers resistance to torques not equal to the commanded steering ratio. In experimentation by Kim perpendicular torque is applied using a brake on one of the drive rollers. In this simulation we set the desired transmission angle to 45 degrees, a 1:1 ratio while commanded input drive roller speed range is 10 to 100 rpm. A brake torque ranging from -0.5 to 0.5 Nm is applied to the output drive roller and the output speed is recorded for each input speed and brake torque. The actual transmission angle is calculated, followed by the sideslip angle, α , using equation 2.

$$T = \tan(\gamma + \alpha)$$

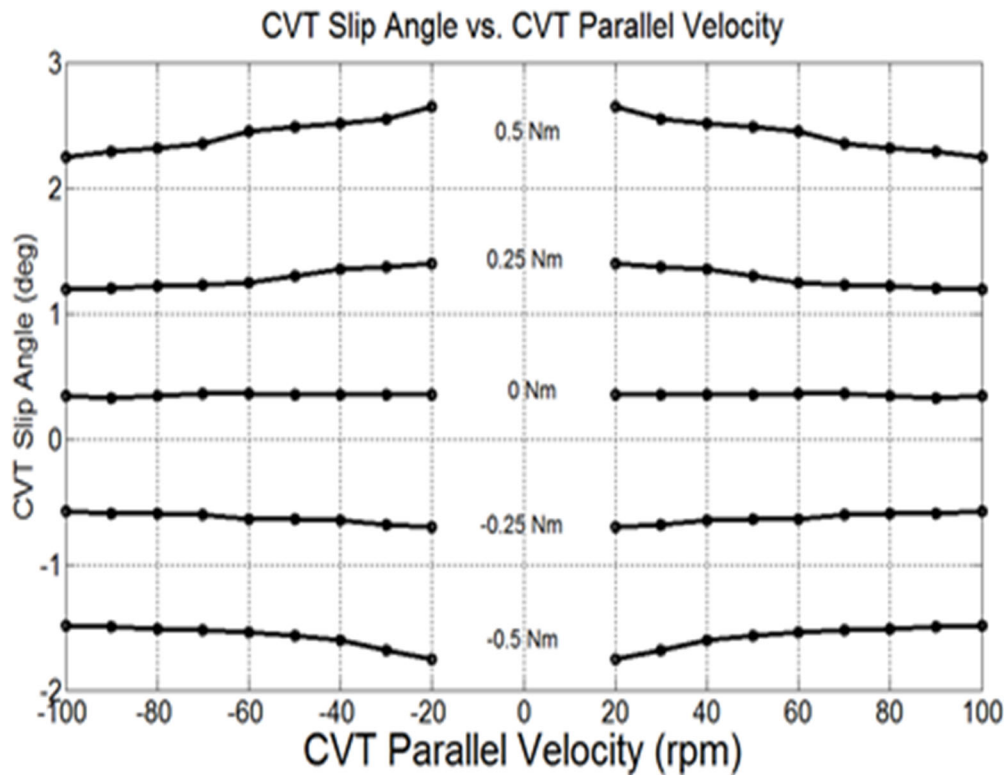


Figure 6: CVT velocity negligible to CVT operation performance

The simulated results are displayed in Figure 6. As can be seen, ADAMS produces results that correlates to the trends shown by Kim calculating the sideslip angle of a tetrahedral CVT. Both sets of results concur that the sideslip angle is nearly independent of drive roller speed.

Slip Angle Proportional to Load

The last test used to validate the Adams model focuses on how transmission angle affects CVT sideslip angle in the presence of increasing perpendicular torque. The result of perpendicular torque is that the actual drive roller angular velocity ratio is different than the desired velocity ratio described by equation 1 by the slip angle.

In simulation, we command an input drive roller speed of 300 rpm, and iterate the CVT transmission angle from 10 to 75 degrees while increasing the braking torque on the output roller from 0 to 30 in-lbs.

The simulated results from the Adams model are shown in Figure 7. As shown in both experimentation by Kim and simulation the sideslip angle is proportional to the perpendicular torque for all transmission angles.

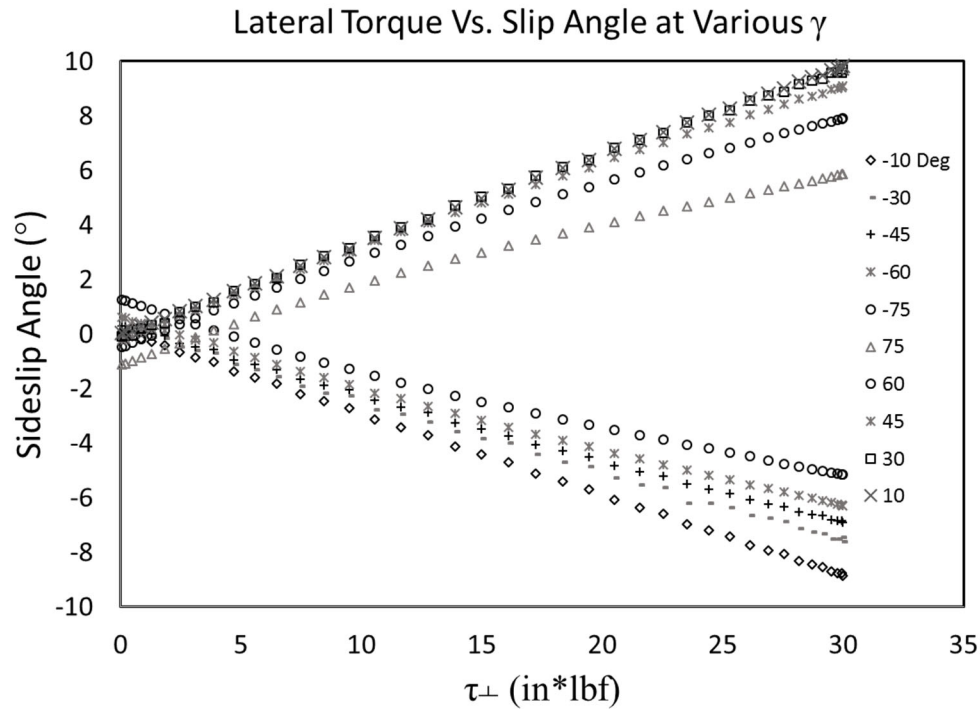


Figure 7: Proportional relationship between sideslip and Perpendicular torque

3.3.2 Box Vs. Tetrahedral Configuration

Kim surmised that a box configuration CVT will perform better than a tetrahedral CVT by reducing the sideslip angle under various loads. This is important because sideslip will degrade CVT performance as it increases, but one should also increase the sideslip a CVT can withstand before gross slip and complete breakdown occur. Figure 8 proves that there is indeed a reduction in sideslip for every transmission angle for the box configuration CVT as compared to the tetrahedral configuration. In fact, the reduction is generally more than twenty percent. Based on this improvement in sideslip, the box CVT will be used in the next section as the primary CVT mechanism of our variable stiffness concept.

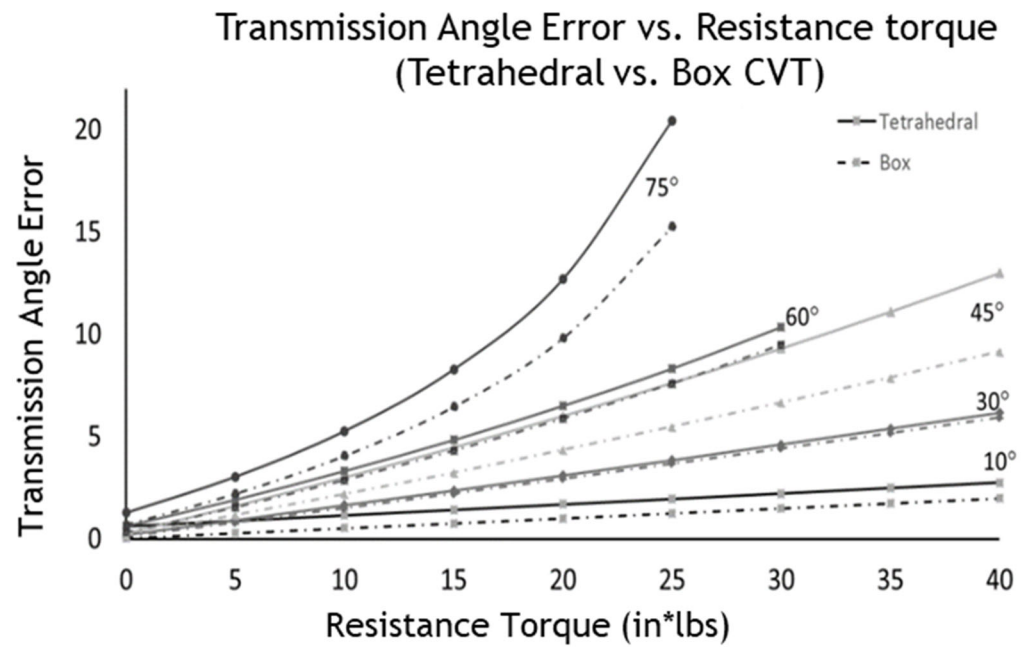


Figure 8: Tetrahedral vs Box Configuration with respect to sideslip

3.4 Variable Stiffness CVT Concept

The variable stiffness CVT is a conceptual device which is a modification of the series elastic actuator (SEA) model shown in Figure 9. A series elastic actuator is generally described as a mechanical system where an elastic element is placed in series with an actuator and its load. The elastic element gives the actuator elastic properties that are useful in many robotics applications.

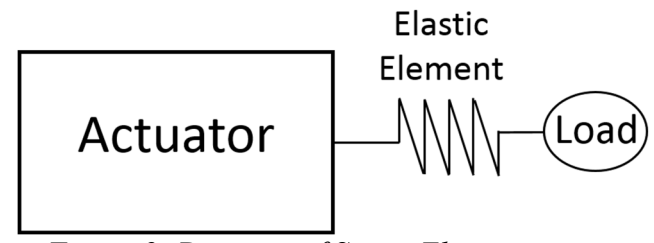


Figure 9: Diagram of Series Elastic actuator

The variable stiffness CVT modifies the SEA concept by adding another component to the system. As shown in Figure 10 in a variable stiffness CVT the actuation element is coupled directly to the load, while the elastic element is coupled to one drive roller of a CVT. The elastic element is attached to the other drive roller (output) of the CVT; since the displacement of the output is proportional to the input displacement based on the steering angle the effective stiffness of the load can be modulated via the steering angle of the CVT.

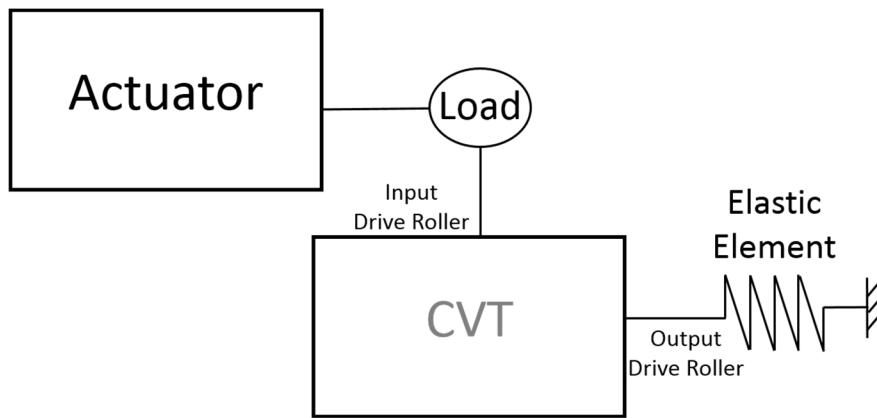


Figure 10: Diagram of the series variable stiffness CVT

3.4.1 Theoretical Variable Stiffness CVT

We understand that an elastic element provides a force or torque proportional to its displacement from equilibrium, i.e.

$$F = k_l x \quad \text{or} \quad t = k_r \theta$$

Achieving variable stiffness with a CVT means controlling the effective stiffness of a working load coupled to the input drive roller via an elastic element coupled to the output drive roller. The effective stiffness is a function of the CVT transmission angle γ . Displacement of the input and output rollers (θ_1 and θ_2 respectively) can be described as

$$\Delta\theta_1 = \omega_1 \Delta t$$

$$\Delta\theta_2 = \omega_2 \Delta t$$

Combining equations 1, 5 and 6 yields the displacement of the output roller as

$$\Delta\theta_2 = \Delta\theta_1 T$$

The torque of a spring on the output roller of a CVT is coupled to the motion of the input roller. By combining equations 4 and 7 the output roller spring torque is related to the motion of the input roller, and the spring torque from the output roller is

$$\tau_{spring} = k_r \Delta\theta_2 = k_r \Delta\theta_1 T$$

It is evident from equation 8 that the spring torque of a CVT can be controlled via the CVT transmission ratio, T . Varying the transmission ratio varies the output roller spring stiffness creating a variable effective stiffness on the input roller that is attached to the working load. The torque applied by the spring is applied to the output roller of the CVT. The effective torque that this spring applies to the working load is transmitted through the sphere to the input roller. The effective torque τ_1 applied to the input roller is calculated based on the transmission ratio of the CVT. The torque relationship is shown in equation 9

$$T = \frac{\tau_1}{\tau_2} = \tan(\gamma)$$

Plugging equation 8 into 9 gives the effective spring torque applied. This is the torque applied to the working load in which the variable stiffness CVT is coupled.

$$\tau_1 = k_r \Delta\theta_1 T^2$$

Equation 10 shows that the effective spring torque is related to the CVT transmission ratio squared. Based on this equation, with a single spring attached to the CVT output, the effective stiffness applied to the load can be varied over a continuous range within operating limits by controlling the CVT steering angle.

The kinematic relationship between the input motion and output spring shown in equation 10 is accurate; however, the actual kinetic response of the system must consider rolling mechanics and the friction losses mentioned in the previous sections.

3.5 Variable Stiffness CVT Application

We have shown Adams to be an effective tool for simulating the CVT dynamics. To demonstrate the variable stiffness CVT concept, we model a 1D legged hopper in Adams based on a study by Miller et al. [4]. In the study, Miller investigates leg adaption to changes in terrain stiffness. The range of leg stiffness needed to adjust between soft and hard surfaces is determined to be between approximately 1.9 kN/m and 2.4 kN/m.

Using the parameters from Miller's study, we recreate the hopper, constrain it to vertical motion and couple the leg to our variable stiffness CVT model. The CVT is equipped with a torsional spring on the output side. The torsional spring is the secondary spring, k_2 , which is in parallel with the primary spring, k_1 , of the hopper. These 2 springs in parallel combine to create a variable effective stiffness k_{eff} ,

$$k_{eff} = k_1 + k_2$$

The secondary spring stiffness, k_2 , is a function of the input displacement and CVT transmission ratio. The effective value of k_2 is calculated as

$$k_2 = \frac{\tau_1}{T^2 \Delta\theta_1}$$

It is of note that in equation 12 the input torque τ_1 is used to calculate k_2 even though the secondary spring is not directly coupled to the input.

The design parameters used in the simulation are listed in Table 2. The CVT is coupled to the 1D leg via a linear to rotational gear transmission. A step input vertical force of 0 to

130 N is applied to the leg over a 1 second duration. The amount of force applied to the system is based on the reverse calculations using spring deflection ranges during contact highlighted by Miller et al., along with the listed hop height and leg mass.

Table 2: 1 legged hopper with variable stiffness CVT Simulation Parameters

Leg Mass	2.16 kg
Linear Spring Stiffness	1.9 kNm-1
Sphere Radius	12 mm
Drive Roller Radius	4 mm
Sphere Material	Steel
Drive Roller Material	Steel
Steering Roller Material	Steel
Torsion Spring Stiffness	1 kNm / deg
Static Coefficient of Friction	0.7
Dynamics Coefficient of Friction	0.1

3.6 Simulation Results

In Figure 11 the linear displacement of the hopper leg is plotted versus the input force applied to the leg. This displacement is plotted over a range of transmission angles, from 0 to 70 degrees, at 10-degree increments. With a step input of 0 to 130 newtons over a 1 second interval, the total displacement of the leg is approximately 39 mm with a steering angle of 0 degrees and 12 mm with a steering angle of 70 degrees. The change in system effective stiffness is evident by the diversity of force vs displacement curves slopes.

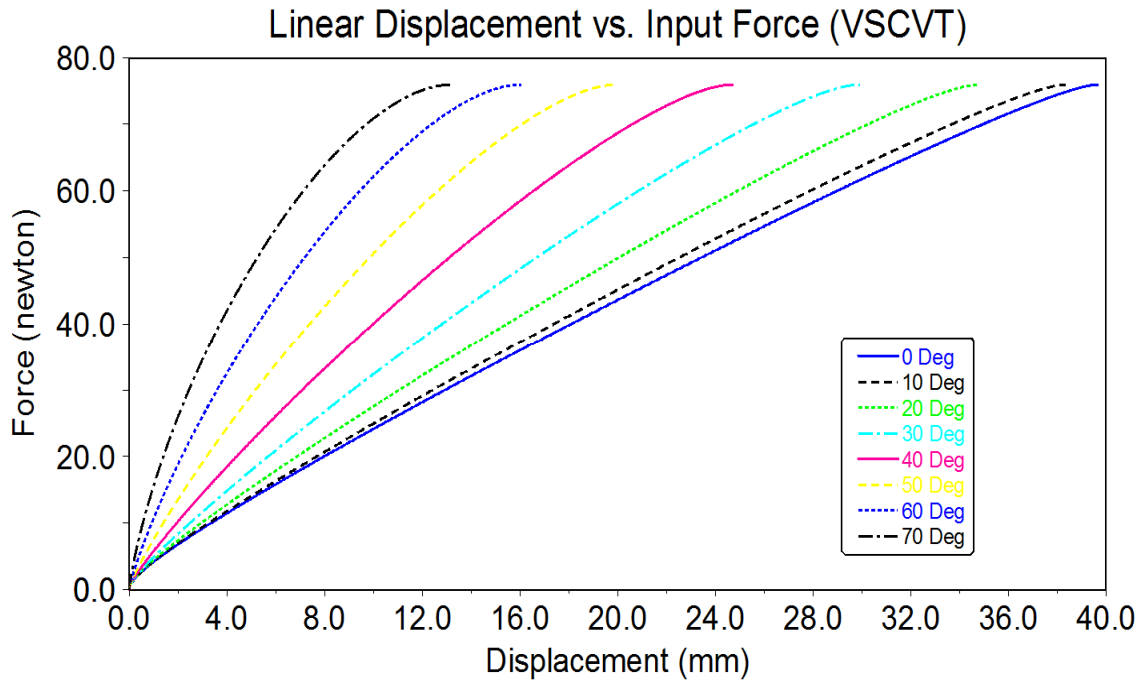


Figure 11: Variable stiffness simulation of VSCVT showing change in displacement by varying transmission angle

Figure 12 demonstrates the ability for a CVT to adjust the effective stiffness of the hopper by varying the transmission ratio of the CVT. The effective stiffness range includes values between 1.9 kN/m and 2.4 kN/m said by Miller to be necessary to traverse both hard and soft surfaces while remaining stable. Importantly, the required stiffnesses are achievable with a transmission ratio of 1:1 (transmission angle = 45 degrees) or less, which reduces the deflection angle of the torsion spring coupled to the output drive roller. This is important in real-world applications, as most torsion springs have a limited range of motion.

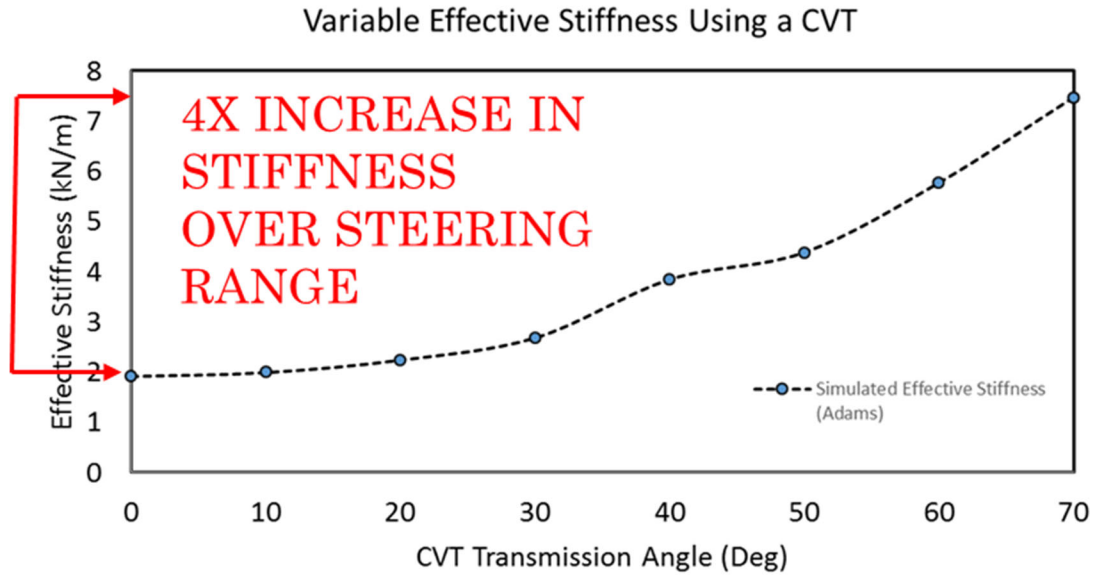


Figure 12: Variable stiffness values using a CVT at various transmission ratio. a 4x increase in stiffness is achieved over the transmission operation range

In this section of the dissertation we presented simulations to prove that a spherical CVT can be used as a variable stiffness device. First, we proved that an Adams model of a CVT compares well with established experimental results. We also presented simulation results showing that the box configuration improves CVT performance by reducing the sideslip angle. We described the use of a CVT as a variable stiffness device and presented simulation results for a 1-d legged hopper equipped with a variable stiffness CVT.

CHAPTER 4

ROBOTIC-SCALE CVT DESIGN

The operating principles of a spherical CVT are very attractive to robotic locomotion applications requiring high-variability in task requirements. If the theory can be expanded to running hopping and walking, the use of CVT can be another step towards mimicking biological systems. The challenge with using these CVT's for mobile robotic applications with dynamic tasks is their overall size, weight and potential limitations in the operational bandwidth of the device.

In order for a VSCVT to be a viable option for variable stiffness mechanisms in robotics is to make sure it can be designed under size and weight constraints making the device suitable for mobile applications. The CVT scale lends to the limitations of component selection and structural design, which inherently will dictate the limitations of the Variable Stiffness CVT operation. With this in mind, we first establish the overall size constraints of the CVT and decide on the working components size and materials accordingly.

4.1 Geometric Scaling

The CVT described in chapter 3 provide the operating principles for the development of the desired variable stiffness device, but these CVTs are much too large for bio-inspired robotic locomotion applications, especially for smaller platforms. Therefore, our next objective is to redesign the CVT for a suitable scale which is nearly ninety-eight percent smaller than many previous designs.

Many experimental robotic locomotion platforms are built on the millimeter scale where components measure between 1 mm and 100 mm in any direction. This makes a CVT that is 50mm on any side a more favorable candidate to be mounted on mobile platforms, whether they are legged, wheeled or aerial, which is required for the hopping application presented in chapter 5. In Figure 13 this milli-meter scale CVT is shown next to a CVT used in previous haptic related robotics research developed by Peshkin et al [32].

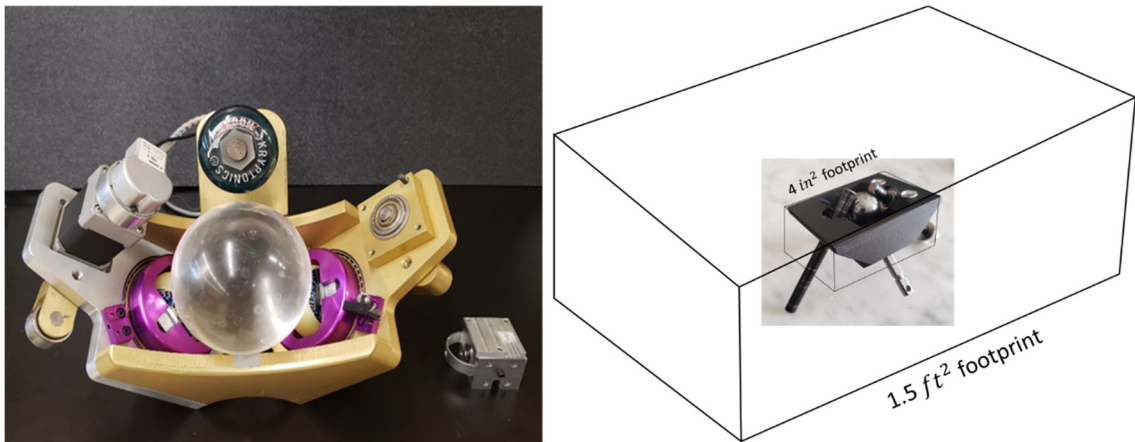


Figure 13: Size comparison of current CVTs to small-scale CVT for Variable Stiffness

4.2 Alignment by Part Reduction

The spherical CVT consists of multiple working components in specific locations relative to each other, creating kinematic relationships that define the operating principles. Alignment is a critical parameter in CVT kinematics. The theoretical relationship between the input roller and output roller of a CVT,

$$T = \omega_2/\omega_1 = \tau_1/\tau_2,$$

is an ideal relationship between the CVT input and output drive roller angular velocities. The relationship assumes point contacts between the transmission sphere and all of the

rollers and that the point contacts positions do not deviate during CVT operation. If the position of any of the rollers is allowed to deviate, which alters the point contact locations, the transmission ratio equation will not hold and the relationship between input and output drive roller will become indeterminate.

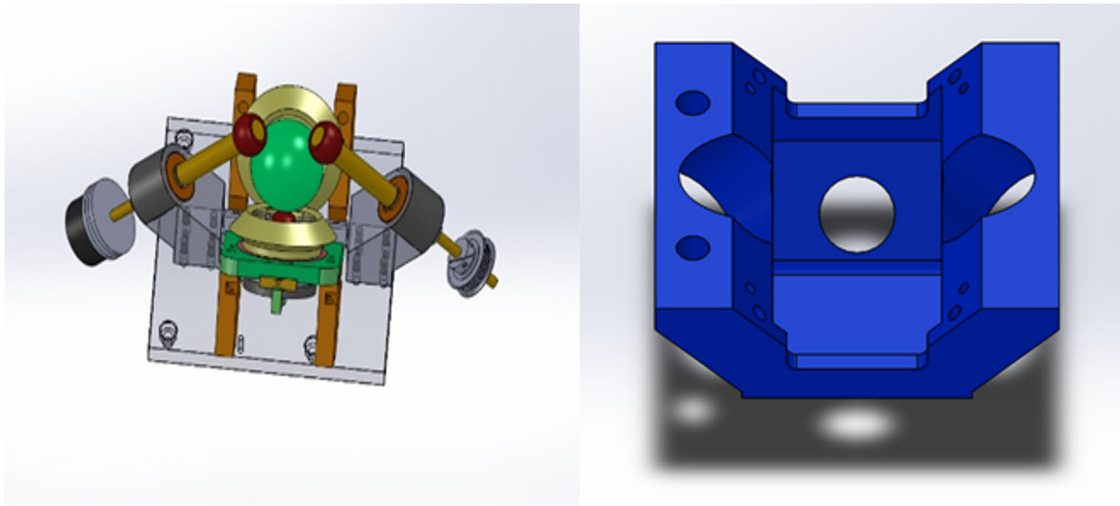


Figure 14: Reduction in number of parts to house the working parts of the CVT

To minimize the likelihood that the rollers will be displaced from the intended positions around the transmission sphere, we must try to minimize the stack-up error in the CVT components design and assembly. In a previous CVT design shown in Figure 14a, there were 11 interconnected components in the support structure. Our redesigned support is a single part shown in Figure 14b. We designed the new support with all the features needed to hold the steering and drive rollers in their proper position around the transmission sphere.

The reduction in the design from 11 parts to a 1 part for the CVT support addresses 2 important considerations of the at this scale, overall size and component alignment. The reduction in number of mating parts and fasteners reduces the stack-up error associated

with mating multiple parts together. This also beneficial to reducing weight by eliminating the need for any fasteners.

4.3 The CVT Contact Patch

The tetrahedral CVT is essentially a sphere caged by 4 contact points, transmitting power from between the input the output drive rollers. It would be ideal for a roller to contact the sphere at a single point; however, when the rollers are pressed in on the sphere the contact points become contact patches. The size and shape of the contact patch is a function of the shape of the components that are in contact, the magnitude of the preload force which presses the rollers onto the transmission sphere and the material properties or all of the rolling components. The size of the contact patch is important because of the adverse effects it can have on CVT performance and lifespan of the working components.

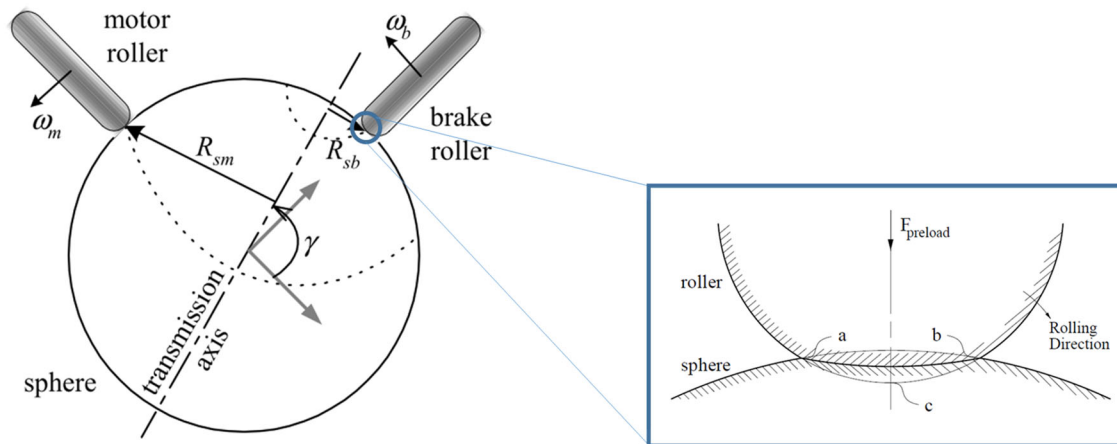


Figure 15: Visual representation of the deformation of materials in rolling contact under some preload force.

The friction force between the drive components of the CVT transmit the power, such that the power transmitted is a function of coefficient of friction and the normal force (in this

case preload force). The size of the contact patch is also a function of the normal force - more normal force leads to a larger contact patch. While the increase in normal force allows for more power transmission through the CVT, as the contact patch increases more friction force exists outside of the “contact point”. This friction creates a shearing force in each rolling contact that degrades the surface of the rolling components and resists ideal rotation between the sphere and drive rollers.

The presence of the forces in the contact patch induce shear forces on the rolling components in contact when the CVT is operating. These shear forces are present at all roller contacts, but are especially of concern at the drive roller contacts. The roller axis of the transmission sphere is never parallel to both drive rollers simultaneously; therefore, shear forces are always present and a threat to material integrity.

As shown in Figure 16, softer metals do not have the surface strength to resist the withstand the shear force under the preload required to transmit power.

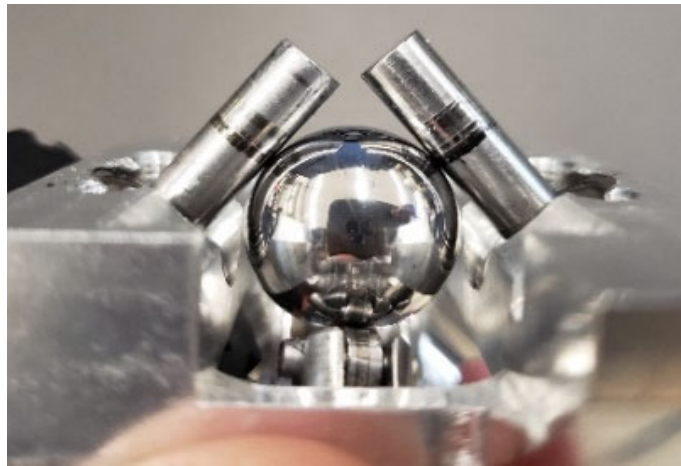


Figure 16: Wear on roller shafts as a result of the shear forces in the contact patch

The shaft material degrades rapidly, causing misalignment in the CVT and thus a reduced level of performance of the CVT. This is a result of the forces within the contact patch. Therefore, the material selection for these contact components should consider reducing contact patch size, resistance to shear/material wear.

4.4 Material Selection and Customized Components

The spherical CVT is comprised of 5 working components that interact with each other normal force and dry friction. For larger CVTs the material properties of these components is not a major concern because of the lack of size restrictions. As the CVT is scaled down, the forces necessary to allow power transmission can exceed the forces the components can withstand at the smaller scale. Therefore, when designing a smaller CVT specific material characteristics and geometric constraints need to be considered for each of the components. These considerations are presented for each of the working components of the CVT.

4.4.1 CVT Custom Support

The initial iteration of the CVT was designed with 2 objectives. The first objective is to maintain the alignment of the working (rolling) components of the CVT. The second objective was to reduce the weight of the support. At this scale the trade-off between the material weight and strength must be considered. There are a number of options to be considered, but for this research only 3-D printed ABS plastic and lightweight metal CVT supports are compared for a direct correlation of the weight vs. strength trade-off.

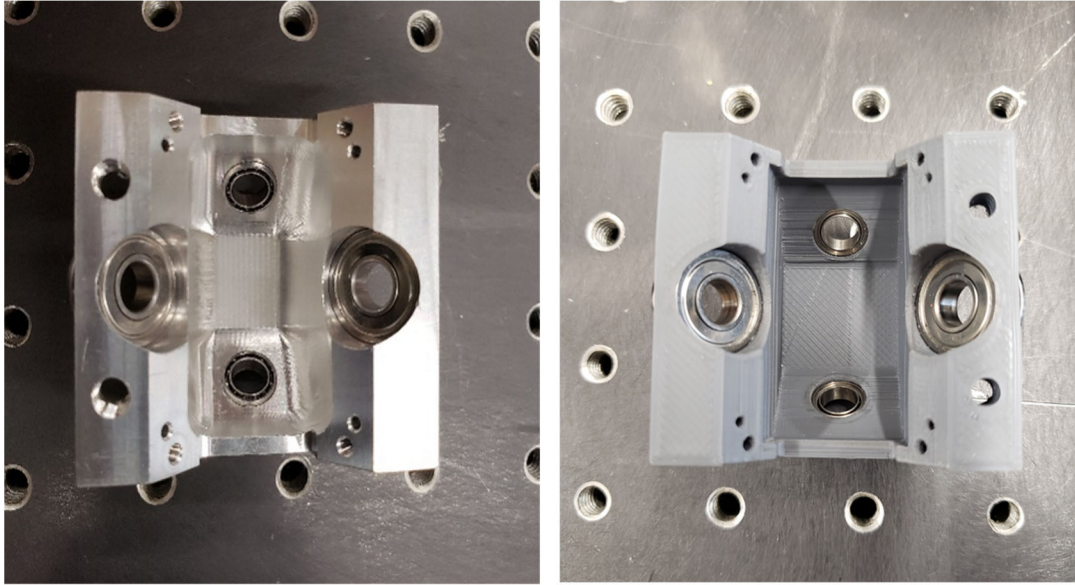


Figure 17: Left is an aluminum CVT support, and at right is a 3D printed ABS CVT support, both have bearings inserted into the provided housings.

The CVT support is under stress in various directions. The drive roller bearings are under radial loading while the steering roller bearings carry thrust forces. In the tetrahedral configuration of a CVT these forces all act on separate face planes of the support. This introduces several deformation surfaces and vertices, which can be detrimental to the alignment of CVT components if the CVT components, support material or bearings is not sufficiently strong.

4.4.2 Transmission Sphere

The transmission sphere is the core component of a spherical CVT. It is the central component of the device, aligning the drive and steering rollers and transmitting power across the device. The sphere radius is the first geometric dimension used to determine the dimensions of the other working components, which have relative radii. A design constraint for the diameter of the sphere was imposed to aide in the general component

selection; sphere diameter less than one-half the overall length of the CVT footprint. For this design the sphere diameter is required to be less than 1 in because of the 2 in target size for the length of the CVT.

For a CVT at this scale the transmission sphere has 3 primary material properties that are most relevant to successful operation; a surface hardness to resist the wear from twisting shear forces in the contact patch, minimal deformation under compressive loading to reduce misalignment of the sphere and/or rollers, and frictional properties between the transmission sphere and the drive rollers. In Figure 18 a diagram highlighting the forces acting on the transmission sphere during operation.

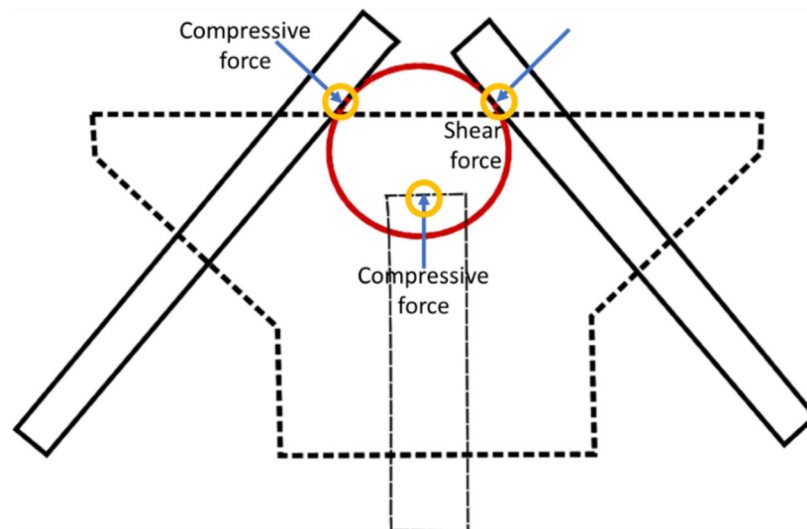


Figure 18: Diagram of forces of interest acting on the transmission sphere in a spherical CVT

Different classes of materials were experimentally tested and measured against each other. A number of these spheres are shown in Figure 19. Spheres ranging from firm rubbers to

hard metals with varying material properties are compared based on the maximum working transmission ratio and maximum transmitted torque. The final choice for the sphere material was tungsten steel.

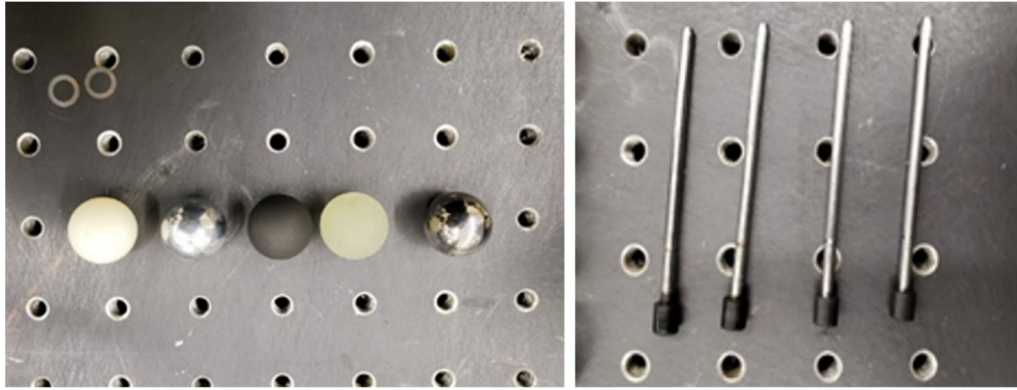


Figure 19: Multiple Materials of Spheres and Drive Rollers for Comparison as CVT working components

4.4.3 Drive Rollers Selection

In this VSCVT prototype, where minimal size and weight is a priority, the drive rollers have multiple functions. Besides power transmission, the drive rollers must withstand the bending moment from the preload force to keep the transmission sphere centered within the VSCVT. Also, the input roller is used to couple the robotic mechanism to the CVT, which means the design must allow access to the input roller.

When the CVT is fully assembled, the drive rollers experience a cantilever bending moment from the preload force exerted from the steering rollers. There is also shearing forces present in the contact patch where the drive rollers contact the transmission sphere.

A visualization of these moments and forces are shown in Figure 20.

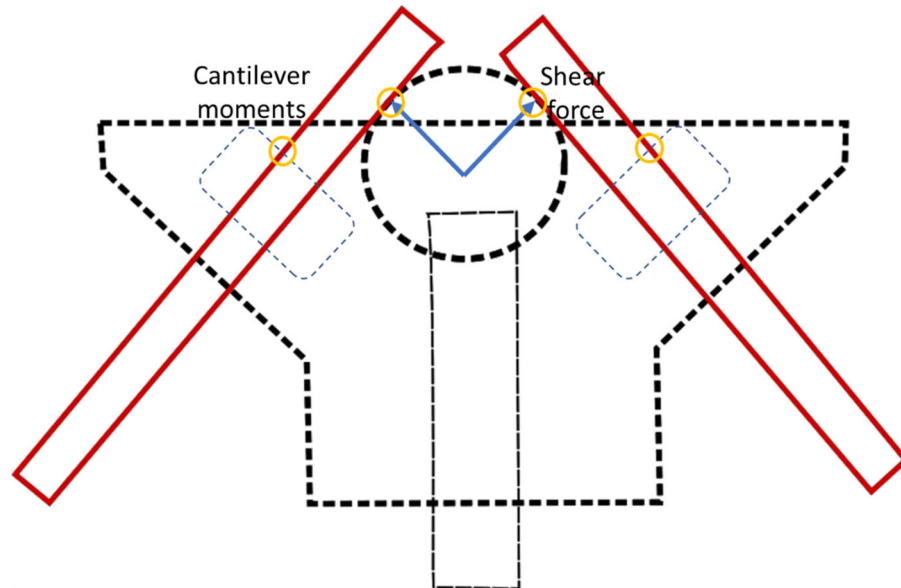


Figure 20: Diagram of forces of interest acting on the drive rollers in a spherical CVT

The material selection for the drive rollers is intended to resist the shear forces causing material wear and the cantilever moments causing roller bending. Both of these effects are detrimental to the CVT operation because they will allow misalignment of the CVT components. Therefore, for drive roller material selection the most important properties are material surface hardness and bending stress. We chose shafts with larger diameters to resist the bending moment and we chose steel shafts for higher surface hardness. Our final choice was a 1/4" diameter black carbon steel drive roller shafts. We also tested steel shafts coated with rubber surfaces for increased traction and power transmission, but the current manufacturing processes are not capable of producing rubber coatings that can withstand the shear forces without tearing.

4.4.4 Steering Rollers

In a spherical CVT the steering rollers regulate the orientation of the sphere's rolling axis and apply preload to all rolling surfaces. These 2 functions require that the steering rollers have the ability to roll freely against the transmission sphere and rotate to adjust the transmission angle of the sphere. A design of the steering rollers that meet these criteria is detailed in the remainder of this section.

The steering rollers need to roll freely with negligible resistance. The steering rollers in this CVT are $\frac{1}{4}$ in high-speed radial bearings mounted on $\frac{1}{8}$ in steel shafts. These bearings are rated for 240 lb. dynamic loading. This steering roller subassembly is mounted inside of a customized steering shaft. The steering roller shaft is custom designed to position the steering rollers precisely and allow the two degrees of freedom for the steering rollers. The shafts are $\frac{1}{4}$ in in diameter with a hub $\frac{1}{2}$ in x $\frac{1}{2}$ in hub at one end. The $\frac{1}{4}$ shafts have a flat side for use of a set screw when mating with the steering roller gears, which I will cover later in this section. The steering rollers shafts are pictured in Figure 21. A detailed drawing of the shafts can be found in the appendices.

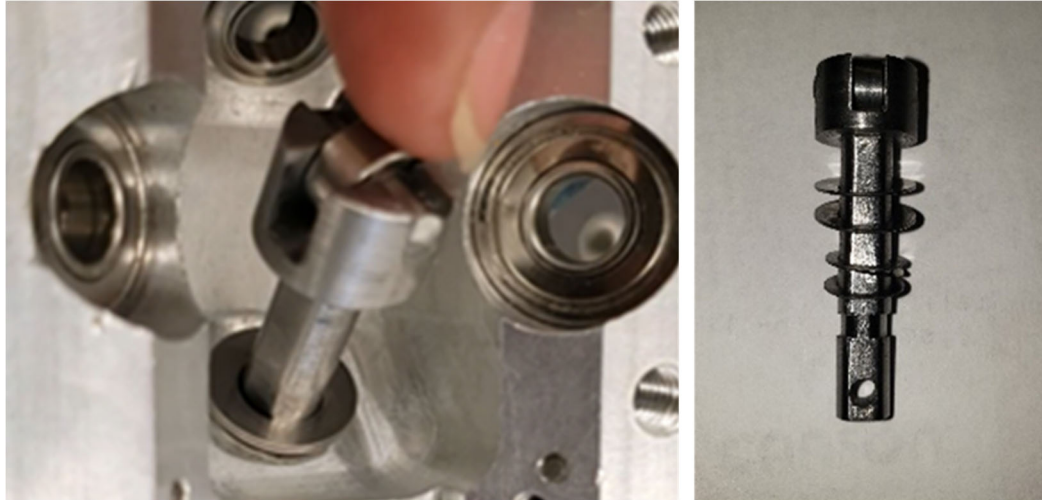


Figure 21: Custom steering roller shafts assembly. The steering roller, steering roller shafts and preloading Belleville springs are pictured here.

The hub of the steering roller shaft has 2 functions. It acts as a mechanical stop for the shafts when they are placed inside of the bearings in the CVT support, but also as a mount for the springs used to provide the preload force to the CVT contact components. The springs are mounted between the steering roller shaft hub and the inner surface of the CVT support body. Belleville disks springs for $\frac{1}{4}$ in shafts are used in inverted configuration as springs to provide the preload force.

These shafts allow for both of the required degrees of freedom; they can translate linearly within their bearings to compress the spring and provide preload to the CVT components and they rotate freely within their bearings, allowing the rotation axis of the transmission sphere to be regulated by changing the angular position of the steering rollers. The steering roller shafts need to be coupled to each other to maintain the required equal and opposite steering roller orientation. For this purpose, oversized spiral miter gears are used to couple

the shafts. The gears help minimize backlash but sacrifice overall CVT size and weight reduction. To compensate for weight the gears are 3D printed.

4.4.5 Preloading Platform

A Custom Preload platform was designed to assemble the CVT and apply preload to the CVT contact components. The tetrahedral configuration CVT requires an oddly shaped support case to accommodate the geometric relationship between component locations and contact points. The custom platform is designed to support the CVT and keep it stationary during the assembly process. The preload platform is comprised of a custom CVT mount made of $\frac{1}{4}$ " thick steel plates welded 45 degrees from the vertical, making the plates parallel to the surfaces of the CVT. This mount is bolted to a solid steel table. The table is as a significantly sturdy anchor for mounting and preloading the CVT components.

The CVT at this scale is designed with small clearances and tight tolerances necessary to achieve proper alignment and avoid any shifting of components during operation. The clearance between the steering roller shaft hub and the CVT support body is only 0.05 in, which provides minimal space for any motion for the transmission sphere once assembled. In order to preload the CVT, Belleville disk springs are mounted in the small space between the CVT support case and the hub of the steering roller shafts. Without the disk springs installed not all four rollers can be in simultaneous contact with the transmission sphere. On the other hand, with the disk springs installed, there is not enough room to install the drive rollers into the support body unless the disk springs are compressed. The small clearances provide reliable assembly but require that a specific process is followed to successfully assemble all the components in the CVT with the preload force needed to

transmit power from the input to output. In particular, to compress the disks springs, an additional mounting plate is bolted to the optical table with a surface parallel to the CVT support face housing the steering roller shaft bearings as shown in Figure 22.

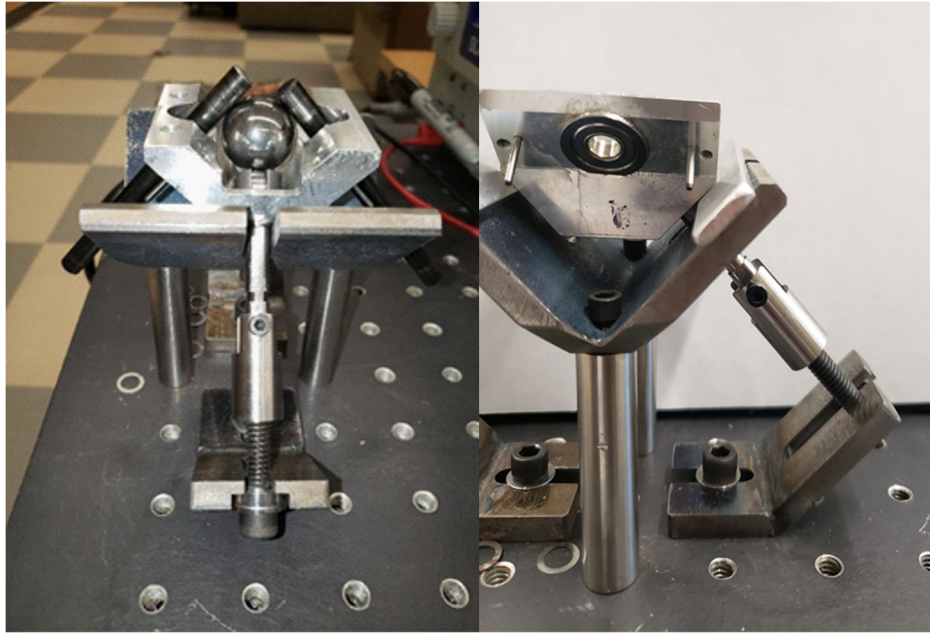


Figure 22: CVT preload mechanism used to assembly the CVT and apply preload

With the disk springs in place between the steering roller shaft hub and the CVT surface, a linear force is needed to compress them. To achieve this force, a custom $\frac{1}{4}$ -20 cylindrical nut is attached to the steering roller shaft using #6 steel bolt and nut. A $\frac{1}{4}$ -20 bolt is screwed into the nut while the bolt head rubs against the mounting plate added to the optical table, shown in Figure 22. When the screw is rotated, it pulls the cylindrical nut and steering roller shaft towards the mounting plate on the bolted to the optical table. This linear motion of the steering roller shaft compresses the disk springs. This process is applied to both steering roller shafts, incrementally compressing the springs until they are flat. Once the disk springs are flat, there exists enough clearance to add the transmission sphere and install the

drive roller shafts. Once all of the components are in place the screws are loosened, allowing the disk springs to expand and apply the preload force needed to align all of the parts and create the traction force needed to transmit power from the input roller to the output roller. The steering roller assembly process is further detailed in the appendices with a visual reference.

4.5 Design Conclusions

This chapter of the dissertation is the detailed design considerations used to select the components for the VSCVT prototype. In Table 3 the physical components of the device are listed. The VSCVT is geometrically scaled to a size allowing the device to be added to an existing robot platform with minimal invasion and design modification of the original platform. The CVT support material is lightweight aluminum for strength and weight considerations. With advancements in 3D printing a support made of a metal infused plastic such as carbon fiber infused ABS printed using the Markforged series of 3D printers.

Table 3: List of the selected components for the VSCVT physical prototype

VSCVT PROTOTYPE COMPONENTS		
Component	Material	Component Details
CVT Support Structure	Aluminum	4 in ² footprint. Details in appendix
Transmission Sphere	Ultra-hard tungsten carbide	$\frac{3}{4}$ in ² diameter
Drive Rollers	Black oxide case-hardened steel	$\frac{1}{4}$ in diameter, 6 in length
Steering Rollers	440C Stainless Steel bearings	$\frac{1}{8}$ in inner diameter $\frac{1}{4}$ outer diameter radial bearings
Drive Roller Bearings	440C stainless steel	$\frac{1}{4}$ in inner diameter $\frac{3}{8}$ in outer diameter
Steering Roller Bearings	440C stainless steel	$\frac{1}{4}$ in inner diameter $\frac{1}{2}$ in outer diameter

The working components of the VSVCT have been selected as hard metals to resist wear and deformation from preloading and operation. The transmission sphere is tungsten steel, drive rollers are case hardened carbon steel, steering roller are steel roller bearings. Finally, the spiral gears used to couple the rotation of the steering rollers shafts are 3D printed from ABS plastic. The overall weight of the prototype is less than 250 grams, 234 grams fully assembled, which is well below the target weight of 300 grams. This is a specific target value to reduce to the tradeoff of added weight to effectiveness of the device.

CHAPTER 5

VARIABLE STIFFNESS CVT

5.1 Introduction

Biological inspiration from animals and humans give the scientist templates needed to develop highly functional robots that can perform human tasks. As the research continues to develop it becomes more evident how significant elasticity can be in all human tasks. The body has elasticity in limbs, joints and the torso and leverage this compliance in different ways depending on task requirements. Zhou states that "biomechanical studies have revealed that all running animals, from small insects to large mammals, generally achieve fast speed by taking advantages of musculoskeletal springs distributed in legs, backs and elsewhere in their bodies." [37]. In current robotics elastic elements have been added to many robots of different types [38] [39] [40].

When focused specifically on legged robots' compliance is not only widely incorporated in robots, but the ability to vary the compliance is being explored more. Often legged robot researchers have varying metrics they intend to examine, but they can be characterized in 2 domains, control schemes or mechanical development. In this research the realization of a variable stiffness mechanism focuses completely on mechanical development.

For this research a CVT coupled with an elastic element to create a mechanically controlled effective stiffness device. To my knowledge, CVTs have not been used to produce a variable stiffness device outside of this research. Peshkin and Colgate explain the principles of spherical CVTs and how they are used to impose virtual constraints in haptic

applications [32]. The principles of operation detailed in that research is expanded to a novel variable stiffness application.

In this research we present a novel mechanism used as a variable stiffness addition to a robotic 1-legged hopper. The novel mechanism, known as the variable stiffness spherical continuously variable transmission, can create a variably compliant elastic element by controlling the transmission ratio between the input and output. Through experimental testing the VSCVT exhibits reliable response to impact forces which are continuous in robot hopping. The VSCVT is then testing in 1D hopping to exhibit the ability to control robotic hopping characteristics by control of the CVT. This mechanism has the ability to address multiple issues in variable stiffness robotics, including low weight and size for field applications, fast stiffness adjustment (order of milliseconds), and simple operation principles. Although the device requires a separate actuator to adjust the stiffness, the actuator torque requirements are quite low, which allow the use of smaller less powerful motors.

5.2 VSCVT Prototype

The novel variable stiffness device presented here is a mechanism based on the design and operation of spherical continuously variable transmissions (SCVT). Details of the VSCVT operation and simulation can be found in the work by Capehart and Moore [5]. The Variable Stiffness CVT is a scaled down version of a tetrahedral CVT suitable to fit the size and weight requirements of mobile robotic applications, specifically legged robots.

Figure 23 is a diagram and picture of the VSCVT prototype. The diagram shows the primary operating components of a VSCVT including the 2 drive rollers, transmission

sphere, 2 steering rollers and the elastic element. The type of elastic element used in this device is shown as a rotational spring in this diagram, but a linear spring is used in the prototype.

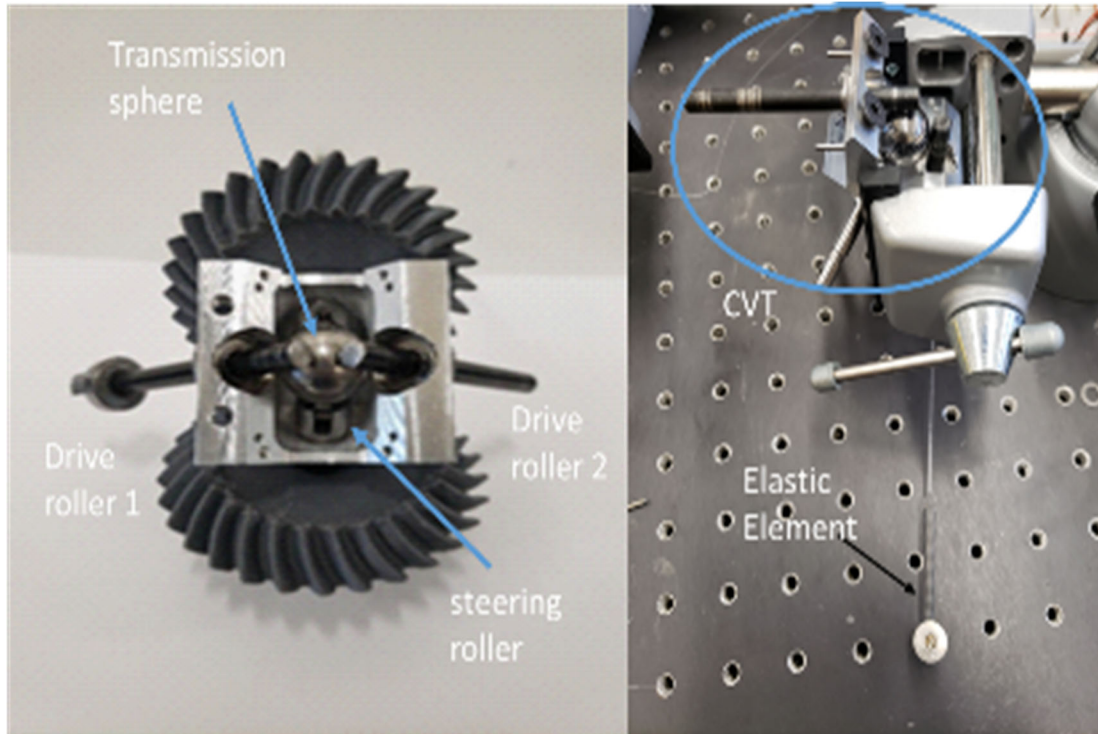


Figure 23: Physical prototype of the small CVT. In the picture to the right the CVT is attached to its elastic element, making the Variable Stiffness CVT

The variable stiffness CVT is a mechanism where an elastic element is coupled to the transmission output and the input is coupled in series to some moving load. The ratio between the load displacement and the output elastic element displacement is modulated by the transmission ratio of the CVT. The control of the transmission ratio controls the effective stiffness of the system as seen by the moving load.

The Secondary spring is coupled to the CVT output and it is the variable elastic element in the system. It's contribution to the system is modulated through the CVT based on the transmission angle between the input and output drive rollers. The ratio between the CVT input and output, T , is regulated by steering angle, ϕ , so that

$$T = \frac{\Delta\theta_2}{\Delta\theta_1} = \frac{\omega_2}{\omega_1} = \frac{\tau_1}{\tau_2}$$

where $\Delta\theta$, ω , and τ are angular displacement, angular velocity, and torque respective, while the subscripts 1 and 2 represents input and output, respectively.

To create the variable stiffness CVT we consider the following. The input to the CVT shall be coupled to the moving load of a focus for the application, i.e. robotic leg, arm, finger, etc. We can denote this input motion as $\Delta\theta_1$. Equation 1 can be rearranged to define the output motion, $\Delta\theta_2$ as

$$\Delta\theta_2 = \Delta\theta_1 * T$$

As stated before the elastic element is coupled to the CVT output. Thus, the stiffness of the elastic element can be described as

$$k_2 = \frac{F}{\Delta\theta_2}$$

where k_2 represents the stiffness of the output spring and F is the external force on the moving load. Substituting equation 2 for $\Delta\theta_2$ we get the relationship between the output spring, input displacement and external load.

$$k_2 = \frac{F}{\Delta\theta_1 * T}$$

From equation for we notice that the output stiffness k_2 is a function of transmission ratio T . The transmission ratio is our control variable thus making k_2 a control parameter, resulting in a theoretically variable spring. The physical spring stiffness is constant, but the effect of the spring on the system which is coupled to the CVT input side has variable stiffness.

5.3 VSCVT Application

To demonstrate the effect of a variable stiffness CVT we apply the mechanism to a 1-legged robotic hopper. One of the characteristics of the VSCVT is the ease of implementation into existing mechanism. To couple the VSCVT to the hopper a simple rack and pinion is used, where the shin of the robotic leg is replaced with a rack and in input roller of the CVT has a pinion attached which meshes with the rack.

Figure 24 is a diagram of the VSCVT utilized in a 1-D hopping application. Once a force is applied to the leg, the legs linear displaced is transferred to rotational motion of the CVT input drive roller, which displaces the spring connected to the output drive roller of the CVT. The effect of this output spring is directly controlled by the CVT transmission angle.

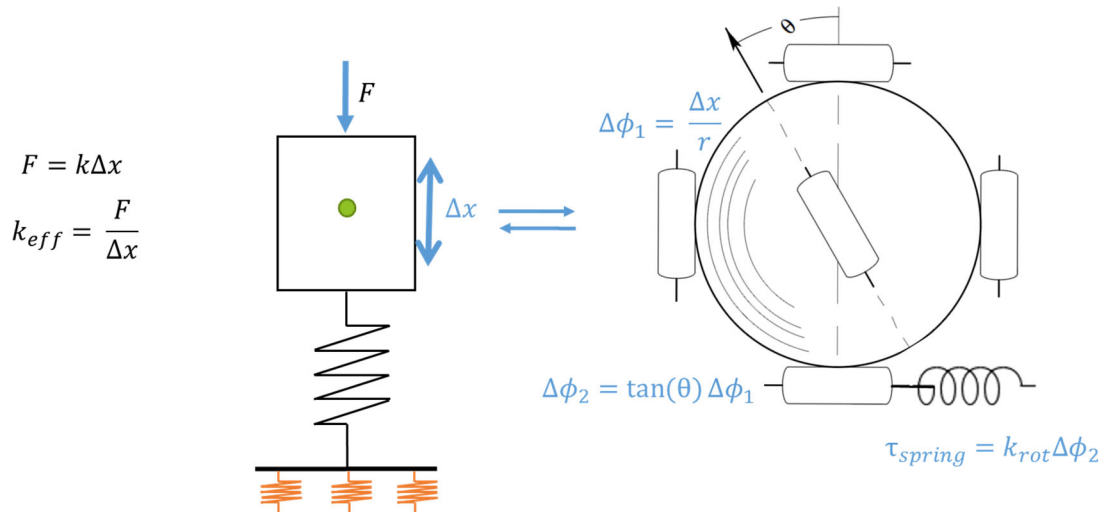


Figure 24: Conceptual diagram of variable stiffness hopping application

To test the theory of this mechanism, the combination of the 1-legged hopper and the VSCVT was first implemented and tested in simulation. Using Adams multibody dynamics simulation software, the VSCVT was coupled to a 1-legged hopper. The hopper performed 1-D hopping tasks to demonstrate the variable stiffness effect possible when the VSCVT is coupled to the leg. In this application there are 2 passive springs in the system. The primary spring is connected to the leg, which was previously the only spring in the 1-legged robot, and a secondary spring connected to the output drive roller of the VSCVT. This secondary spring is in parallel with the primary spring creating a variable stiffness effect for the entire robotic leg as seen in the following equation.

$$k_1 + k_2(\theta) = k_{eff}(\theta)$$

The effective secondary spring stiffness, $k_2(\theta)$, and thus the effective stiffness, k_{eff} , of the system are theoretically a function of the steering angle, θ .

With the system coupled in simulation, we tested in the hopper in multiple 1D tasks relevant to robot locomotion. In the Figure 25a the simulated model of the 1-legged hopper and VSCVT combination in Adams is pictured. The three graphs are the results from three task simulated by the robot leg.

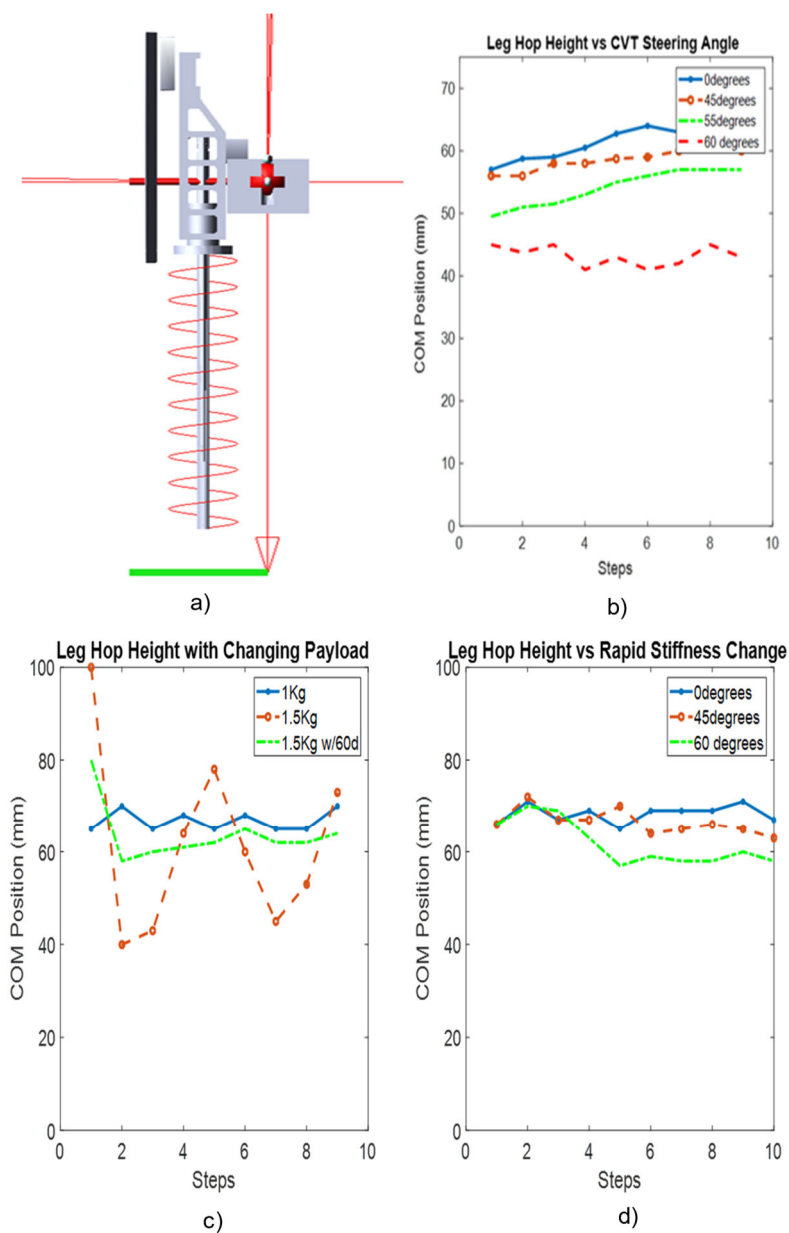


Figure 25: Adams simulation of a variable stiffness 1D hopper performing multiple robotic tasks

In Figure 25b the robotic leg demonstrates the ability to achieve steady state hopping at various hop heights as a function of the commanded transmission angle in the VSCVT. For the 4 different transmission angles there are distinct hop heights achieved by the robot, with a thirty-five percent increase in hop height over the VSCVT transmission range. This is a significant result as it has been said that a robot's ability to change its hop height on a common surface also demonstrates an ability to adapt stiffness to changes in surface stiffness [41].

Figure 25c,d demonstrate performance on more specialized tasks. Figure 25c shows the robot's ability to stabilize itself in the face of an increase in payload. We show that a significant increase in payload will destabilize a robot. To compensate for the increase in payload, animals and humans increase their leg stiffness to maintain stability [2]. The VSCVT gives the robotic leg that same capability to re-stabilize itself with an increase in system stiffness due to control of the CVT transmission angle. In this task a payload increase of fifty percent is stabilized to the baseline hopping behavior. This shows how the VSCVT can be used in a common real-world application.

Figure 25d is similar to the results shown in the top right graph. The distinction is that the stiffness of the leg is adjusted during the flight phase of the robotic leg. In this task, the stiffness of the robotic leg is adjusted between the first and second hop. Notice the deviation in hop height is immediate during the subsequent hop. Within 4 full hop cycles the robotic leg settles to a new steady state. This is the benefit of how fast the VSCVT can adjust the system stiffness, approximately 200 milliseconds to cover the entire stiffness range of the

device. This simulation shows the VSCVT to be very suitable for real-time applications, such as on-board adjustments to terrain changes during locomotion.

5.4 Experimental Validation of Variable Stiffness

The simulated results from Adams show the effect of adding a VSCVT to a robotic leg. As mentioned in section 4.4 a physical prototype of this VSCVT has been designed and built. To test the VSCVT prototype experimental platforms are designed to verify the effective operation of this mechanism in a real-world application. Two different experimental platforms are used for testing. The details of the experiments and the results are explained in the remainder of this chapter.

5.4.1 Impact Pendulum Test

The platform is shown in Figure 26. It consists of a 1D robotic leg mounted to benchtop horizontally and coupled with a VSCVT. The leg is mounted horizontally to isolate the effect of the VSCVT on the robotic leg, while ignoring the complexities caused by the multiple phase changes of a hopping robot. To induce the impact force seen by a robotic leg during locomotion an impact pendulum is set up to provide a consistent and repeatable impact force. This gives us the ability to test the VSCVT in a controlled experiment.

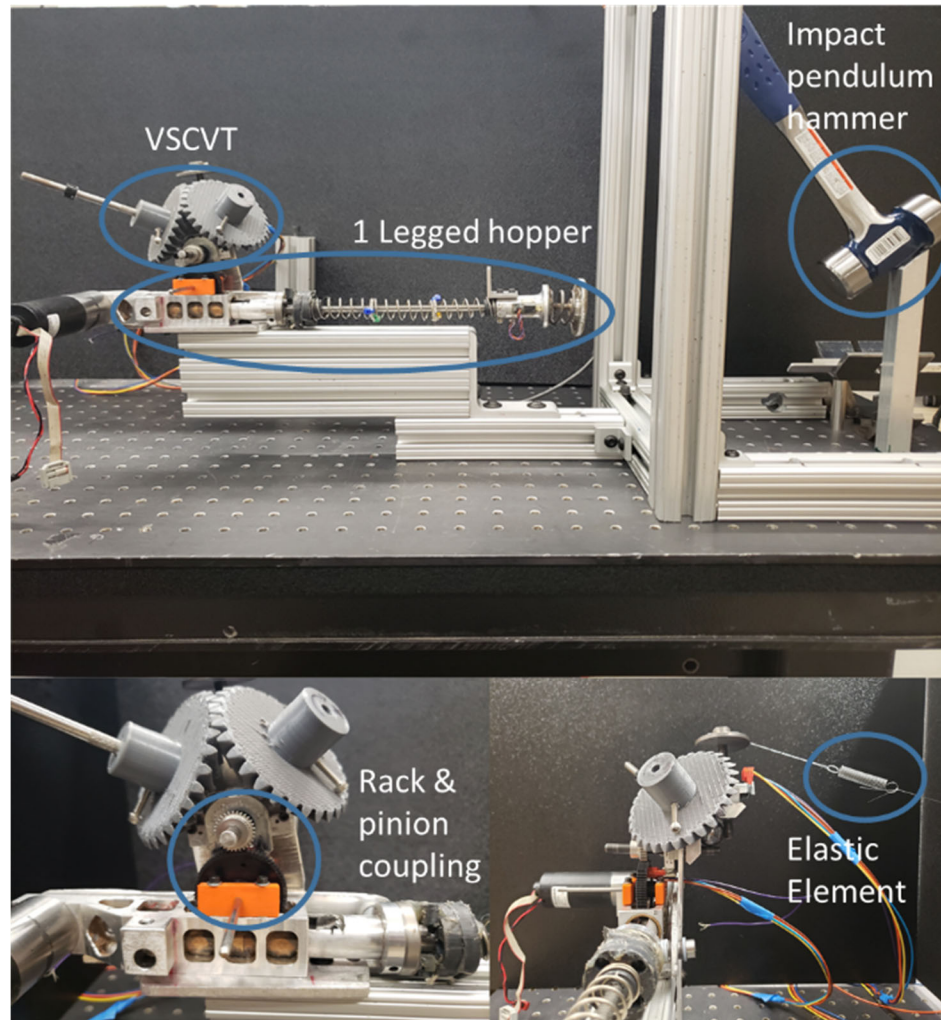


Figure 26: The impact pendulum experimental platform used to test VSCVT response to impact forces of hopping

To test the effect of the VSCVT, we impart an impact force on the leg using the pendulum hammer. This force causes deflection of the robot leg and as the springs absorb and release the energy from the hammer. In theory, as the springs of the system become stiffer the deflection of the leg would decrease if the impact force remains constant.

To show the effect of the VSCVT, the experimental method is as follows. The pendulum hammer is set to its constant starting position and remains at rest until released by user. The VSCVT spring is set to its initial rest length, in slight tension to reduce the chance of slack in the cabling. We then set the transmission ratio of the VSCVT, which is the control variable of the robotic leg's effective stiffness. We set the CVT to different transmission ratios over a range from 0:1 (inactive CVT) to 5:4, which we expect correlates to a change in system stiffness.

To quantitatively validate the change in stiffness we measure the deflection of the leg after impact via an AMT103-V encoder. The pendulum position and VSCVT deflection are also measured using similar encoders. A teensy 3.2 microcontroller is used for data acquisition.

5.4.2 Impact Test Results

The results of these impact test are shown in Figure 27. For each VSCVT transmission ratio, the pendulum hammer was released with 14 Newtons of energy and the deflection of the foot of the robotic leg is measured using the encoders. Each of the pendulum test iterations was performed 8 times and averaged across the trails with a standard deviation of less than five percent.

The graph in Figure 27 shows promising results of the effectiveness of the CVT. As the transmission ratio the VSCVT increases from 0 to 5:4, the effective stiffness increases as shown by the trendline. The stiffness increases from 0.56N/mm to 0.74N/mm over the VSVCT operation range for this application, an increase of thirty-three percent.

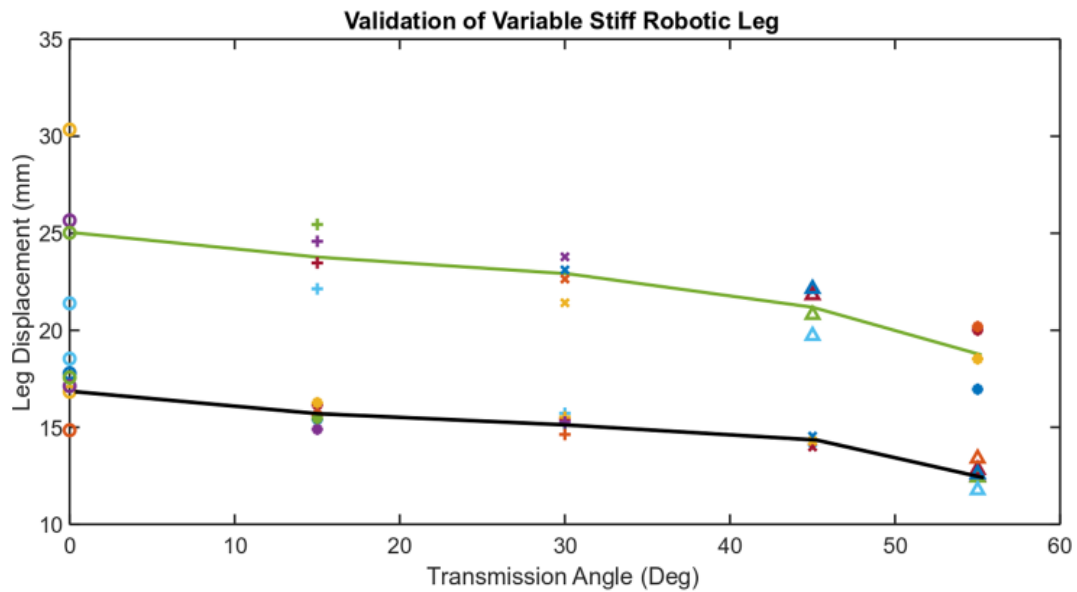


Figure 27: Experimental results of VSCVT response to Impact force using different transmission angles

This is a change in the system stiffness, validating that the VSCVT has a clear effect on the robotic leg stiffness. The value of about thirty-three percent is significant also. Numerical simulations by Miller et.al. state that even when ground stiffness values change over 3 to 4 orders of magnitude, the body only needs to change between fifteen to twenty percent to recovery stability when the surface changes [4]. This is promising for the future application of this device and future iterations of its design.

5.4.3 The Variably Compliant 1-Legged Hopper

In order to validate the effectiveness of a variable stiffness CVT, a 1-legged hopper experimental application is considered. Single leg experimentation is commonly used as a template for studying locomotion and how changes in robot parameters or the environment affect performance. In this application, a robotic legged is coupled with a variable stiffness

CVT and constrained to a 1-d vertical hopping task (It is of note that the VSCVT itself is in no manner designed for this specific application). The combination of the one legged hopper and the VSCVT is known as the VS hopper. The intention of this device is to show the novel ability of the VS Hopper to change the effective sprig stiffness as a function of the CVT steering angle.

The physical prototype of the VS Hopper is shown in Figure 28. It consists of the a one the AER 1-legged hopper with all of its main components coupled with a modular device, the VSCVT. A rack-n-pinion is incorporated via custom 3-d printed ABS mounts to the 1-legged hopper to couple and transmit the motion of the 1-legged hopper spring to the secondary spring controlled by the CVT transmission angle.

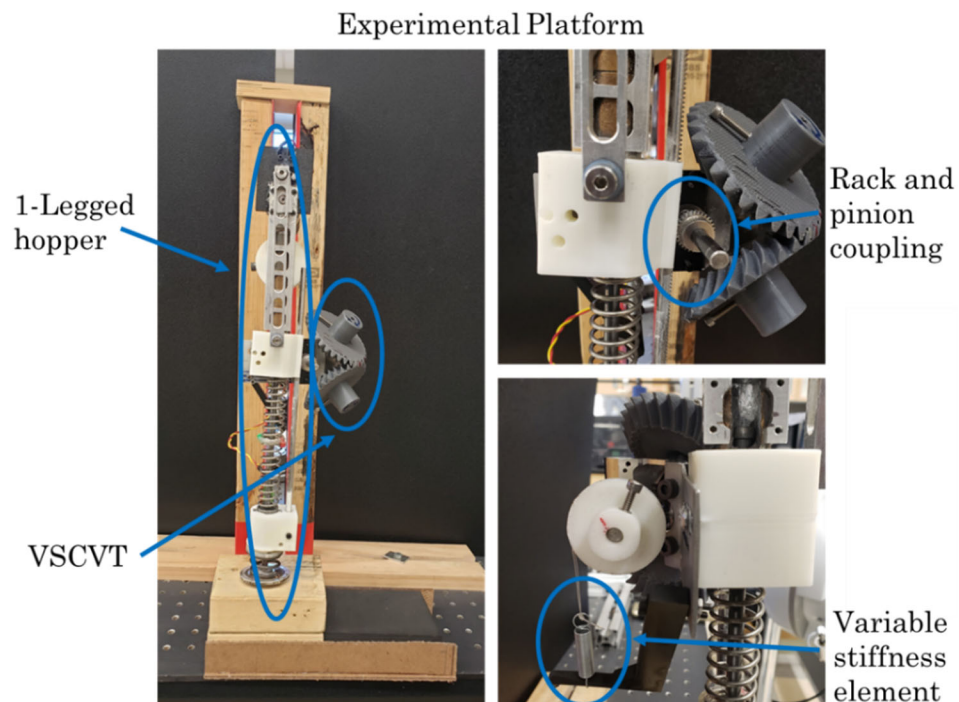


Figure 28: 1-Legged hopper experimental platform used to analyze VS-Hopper. Notice the rack and pinion coupling of the VSCVT and the robot leg in the top-right photo and the elastic element in the bottom right photo.

To test the effectiveness of the VSCVT, the hopping characteristics of the 1-legged hopper are logged and set as a baseline. The VSCVT is then added to run the same test and the relevant changes of behavior in the hopper's performance metrics are considered the measures of effectiveness of the VSCVT.

A Teensy 3.2 microcontroller is used for data collection and actuator control on the 1-legged hopper. A tactile sensor is placed in the hopper foot to detect touchdown, an AMT-v102 encoder at the boom pivot to track the hop height, a reset switch for the AER actuator position. The AER input actuator is a maxon motor with a 63:1 ratio gear head operated at 24 volts. Data is logged to a micro SD card at 1000 Hz. An external ATI force/torque transducer is used to calculate peak impact forces during hopping, as well as extract a true hopping frequency and force profile. A Labview virtual interface is used to set sensor sensitivity and for data acquisition. High-speed imaging is collected using a GoPro optical sensor to collect the visual data to coincide with the numerical data collected from the other sensors in the array. With this small set of sensors, all of the relevant data to exhibit the effectiveness of the VSCVT is available.

5.4.4 Disturbance Rejection on Various Substrates

In current locomotion research 1D hopping can generally be recognized as a trivial task due to previous accomplishments. On the other hand, even in 1D hopping recovery from perturbations and adaptation to changes in terrain characteristics are the focus of a large part of the robot locomotion community. In this section we investigate the effectiveness of the VS-Hopper to aid in disturbance rejection and how the steady state behavior after the

perturbation is affected by the VSCVT setting. The hopper was commanded a feed-forward energy injection scheme to achieve steady state hopping on wood. A 2in perturbation is introduced while the hopper is in flight. This perturbation is about twenty percent of the nominal leg length of the hopper. For robustness and repeatability conformation this test is performed on 3 different landing surfaces from the perturbation, wood, highly stiff foam and highly damped foam, which are listed in the results section.

The number of steps needed to recover from a perturbation is one of the most straightforward methods of analyzing transient behavior in legged locomotion. This metric of perturbation rejection can be easily applied gives a simple comparison across robotic systems. One major drawback of this metric is that it does not lend any information of the severity of the reaction to the perturbation. Number of steps only indicates the recovery time, ignoring the effort required to return to a stable state. With this in mind the number of steps required to recover will be examined along with the decay ratio.

Decay ratio (DR) was presented as one of the stronger disturbance rejection metrics by Miller et al. in their research on quantifying disturbance rejection [42]. The decay ratio quantifies disturbance rejection by characterizing the rate at which a particular gait indicator returns to its equilibrium value following a perturbation. Equation () represents the mathematical representation of decay ratio.

$$\frac{1}{n} \left[\sum_{k=2}^{n+1} \left(\frac{g_k - g_{\infty}}{g_1 - g_{\infty}} \right)^{\frac{1}{k-1}} \right]$$

where n denotes the total number of strides employed, g_k denotes the gait indicator at touchdown, k is the number of strides after the perturbation, and g_{∞} indicates the value of

the gait indicator at equilibrium. In this study the gait indicator used is the apex height of each step. The Figure 29 is a conceptual representation of using apex height as the gait indicator for calculating decay ratio. It was stated by Miller that this metric is advantageous for multiple reasons including reduced number of steps for analysis and flexibility to multiple gait indicators.

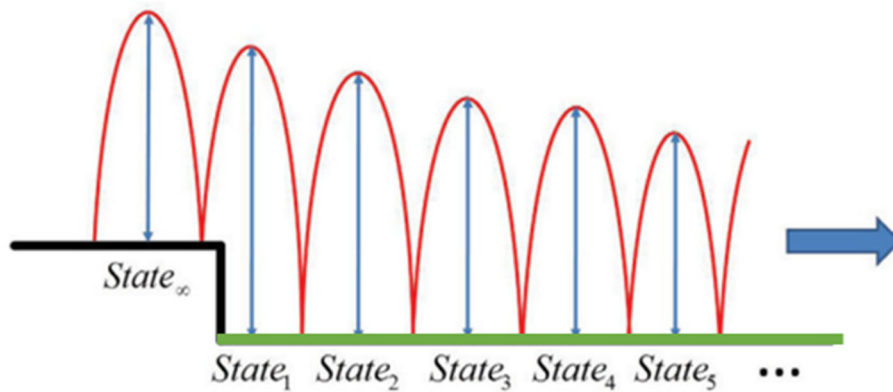


Figure 29: Conceptual representation of Decay Ratio analyzed over a step perturbation

Figure 30 shows a representation of one set of results from the disturbance rejection experiments conducted on the VS-Hopper. This is a result from the twenty percent perturbation landing on a Polyethylene Foam pad, the pad is thick enough to avoid in interference from the solid surface underneath.

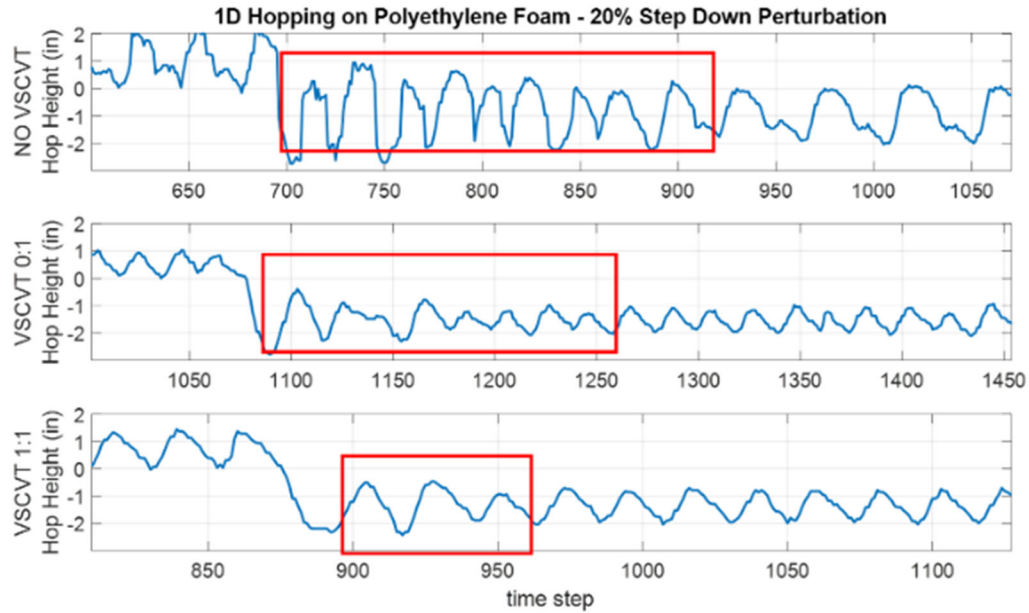


Figure 30: Experimental results of Disturbance rejection testing of VS-Hopper for recovery on Polyethylene Foam surface. Validation of VSCVT as an effective variable stiffness device and shows improved stability by adding the VSCVT.

Notice the improvement in the transient behavior of each graph in the Figure 30. From the top graph to the middle graph there's an improvement in the number of recovery steps. There is a difficult correlation to be noticed for the Decay ratio. The decay ratio increases in some experiments, meaning the transient steps may be more energetic relative to the initial recovery step. The results for this experiment, as well as on the other 2 surfaces are listed in table 1. The combination of recovery step improvement and decay ratio exhibit a very positive effect of the VSCVT as an addition to the hopper. You can also notice an increase in amplitude after the perturbation when the CVT is activated at a higher transmission ratio.

5.4.5 Hop Amplitude Matching on Different Surfaces

When the stiffness and/or damping of a surface changes while a robot is running in 2D gait indicators such as hop amplitude, forward velocity, stability, etc. change as well. This can cause undesired behavior like change slower velocity, unstable amplitudes and often instability to the point of failure. In this 1D hopping experiment we attempted to reject the changes in surface characteristics by showing that we can maintain hopping performance by controlling the CVT transmission angle. For this experiment the gate indicator of concern is hop height. We expected to show the ability to traverse 2 different terrain characteristics and command equal hopping amplitude on both.

The experiment is set up as follows. The 1-legged hopper is equipped with the VSCVT and actuated at a constant input speed. A “hopping surface” slightly wider than the hopper foot is constructed with wood as one surface and a softer material as the other surfaces. The surfaces height did not change during this experiment.

The hopper is powered and allowed to hop on surface one until it reached steady-state performance. Once steady state is reached the hopping surface is moved systematically horizontal in a conveyor-style movement incrementally until the hopper transitions surfaces. In short, the leg hops in 1D and the ground beneath the leg is translated to change the ground characteristics. The hop amplitude is measured throughout each trail continuously using an AMT-103V encoder at the hopper boom pivot. For this experiment, there are six test environments. For each test the ground transition is evaluation the CVT is set to binary setting, one test on and one off.

In Figure 31 the resultant steady-state hop amplitude for the hopper is presented in the bar graph. The surface transition task is performed on three surface sets, softer surface to harder surface and harder surface to softer surface. For each set graph 1 and 2 are with the CVT ratio 0:1. Set 3 and 4 are with CVT ratio 1:1. The second set of hop data clearly indicates the proof of hypothesis for this experiment. In this data set, the first set of bar graphs show a drop of hop amplitude of about sixteen percent when the VSCVT transmission ratio is 0:1 transitioning from the harder surface of wood to the softer/ more damped surface of polyethylene.

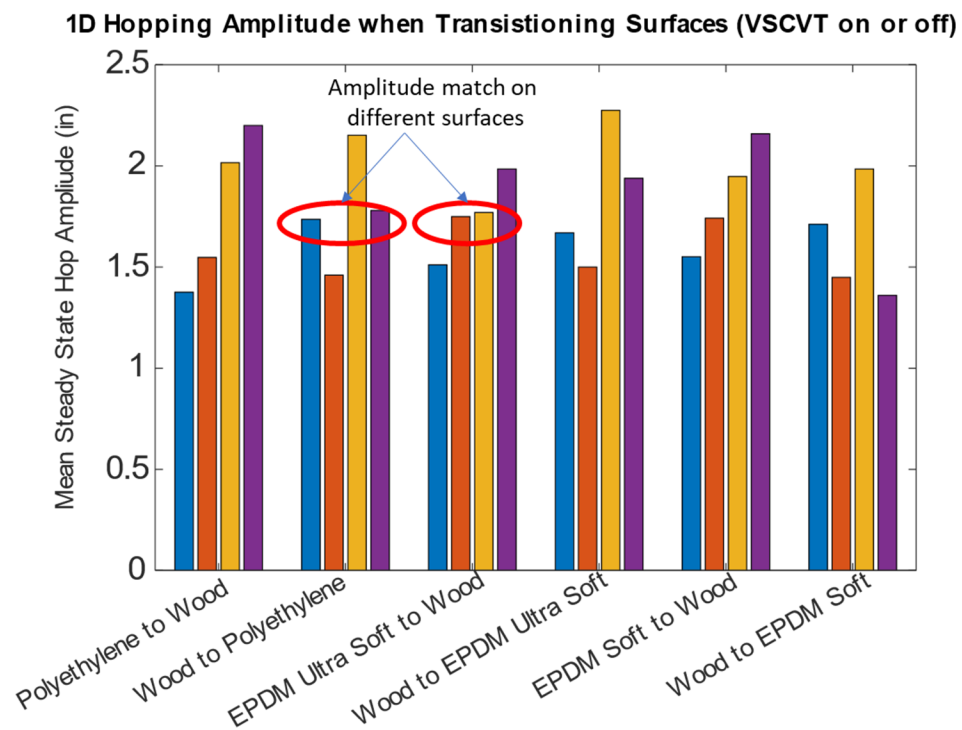


Figure 31: Hopping Amplitude of the 1D hopper on multiple surfaces. It is show on multiple data sets that hop amplitude can be matched on different surfaces using CVT control.

The second set of bar graphs show a similar drop of hop amplitude with the VSCVT angle set to 1:1. The point of focus is that the hop amplitude on wood when the VSCVT transmission angle is 0:1 is almost equal to the hop amplitude on polyethylene when the transmission angle is 1:1.

A visualization of how the hop amplitude will be maintained using the VSCVT is shown in Figure 32 using raw data from the boom hip encoder. Hopping on the wood surface the steady state hop amplitude is 1.76 in with the VSCVT ratio set to 0:1. This amplitude drops to 1.49 in when the hopper transitions to polyethylene. Then, by simply changing the VSCVT transmission ratio to 1:1 the hop amplitude recovers to within one percent of the initial hop amplitude. This is the overall goal of the VSVCT in this task; to maintain hop amplitude on 2 surfaces with significantly different properties by VSCVT control. The hop amplitude can be maintained with less than two percent error by simple VSCVT control, confirming the VSCVT is effective at changing hopping performance on different surfaces, validating the variable stiffness capabilities.

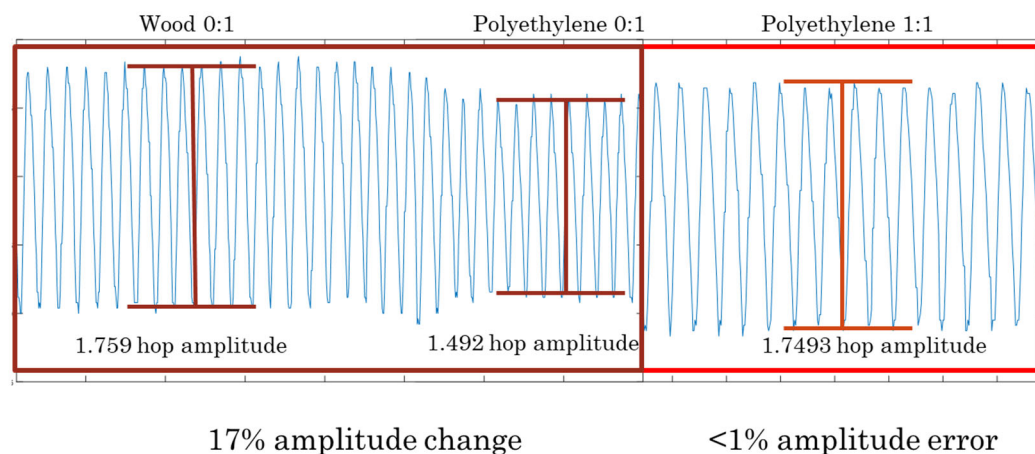


Figure 32: Visualization of hop amplitude matching when transition surfaces by controlling the VSCVT transmission ratio

5.5 Experimental Conclusion

In this chapter the VSCVT mechanism is validated as an effective variable stiffness device in robotic locomotion. It is first shown through ADAMs simulation that the VSCVT can directly control the hop height of a 1D hopper by modulation of the transmission angle. These results led to the final validation of the device experimentally. In the first experiment the VSCVT is tested for response to impact forces in the real world. The VSCVT is able to change the displacement of the pendulum after impact consistently when the VSCVT transmission angle is changed. This is evident in Figure 27.

With the affirmation from impact tests, the VSCVT is tested to show the effect on hopping characteristics. The device is examined in two different 1D experiments, disturbance rejection by traversing a large step perturbation and preserving hop amplitude when transitioning between ground surfaces with different properties. The VSCVT shows promising results in all three experiments. It can be said with confidence that the VSCVT has proven experimentally to be a capable variable stiffness mechanism for locomotion using legged robots.

CHAPTER 6:

CONCLUSION

This dissertation is intended to present the development of a universal variable stiffness mechanism for robotic applications. The application of choice for the proof-of-concept is 1-D hopping of a robotic leg in the face of large step perturbations and changes in surface characteristics. To achieve a physical prototype of the proposed mechanism a multi-step research process was conducted. A large-scale reduction of the spherical CVT was considered through simulation. The results from these simulations provided analytical confidence in the CVTs operational reliability at the required scale for robotic legged locomotion. Simulated results were focused on the operation of the CVT in an idealized situation; not considering the physical limitations of actual design and construction of the CVT. For this reason, the dissertation focuses on the how and why behind component selection and the design considerations involved in creating an experimental prototype of the VSCVT. This set of material and component selection guidelines will help develop variants of the mechanism to meet requirements of a variety of robotic tasks.

The realization of the CVT prototype led to experimental implementation of the VSCVT. Impact testing of the VSCVT using an impact pendulum validated the use of the CVT as a variable stiffness mechanism. The results demonstrated that the stiffness of the VSCVTs elastic element is directly related to the transmission ratio set by the CVT steering angle. Finally, an investigation of 1D hopping on various surfaces was completed. We first attempted steady-state hopping on the different surfaces, analyzing metrics such as steady state apex height, hop frequency and deviation in hop height. We also investigated the

hoppers performance when transitioning between two different terrain types. The last test conducted was the hopper's response to large perturbations caused by traversing an elevation change of twenty percent. The VSCVT shows a positive contribution to locomotion in all three tasks evaluated, proving that the novel device is a viable one for robotics research in related bio-inspired applications.

The dissertation chapters include:

1. Simulated results of the spherical CVT designed on a millimeter scale in comparison to large scale CVTs - Chapter 3.
2. The design process and critical considerations for VSCVT design, including material and component selection - Chapter 4.
3. Experiments with the VSCVT including response to impact force and 1D hopping performance on multiple surfaces - Chapter 5.

6.1 Future Work

While this dissertation set guidelines and outlines the trends to be considered during component and material selection, the process has not been optimized. Improvements in materials, geometries and weight reduction techniques, etc. can lead to an even more functional mechanism, expanding the application possibilities. The mechanism was designed to be adapted to multiple applications with minimal design effort. In the future, the VSCVT can be tested experimental in various robotic applications to verify the robust concept and design of the VSCVT. An automated CVT is the most impactful future research for the current mechanism presented here. With conceptual development and component

selection completed, automation of the steering controls is a design tasks, only requiring the implementation of a computer controlled steering actuator. In closing, this dissertation details the VSCVT and lays the groundwork for promising contributions it can make to robotic locomotion.

REFERENCES

- [1] G. Pratt, M. Williamson, P. Dillworth, J. Pratt and A. Wright, "Stiffness isn't everything," in *Experimental Robotics IV*, vol. 223, Springer Berlin Heidelberg, 1997, pp. 253-262.
- [2] R. Alexander, *Principles of Animal Locomotion*, Princeton University Press, 2003.
- [3] B. Andrews, B. Miller, J. Schmitt and J. Clark, "Running over unknown rough terrain with a one-legged planar robot," *Bioinspiration and Biomimetics*, vol. 6, pp. 1-15, 2011.
- [4] B. Miller, D. Cartes and J. Clark, "Stiffness Adaptation for Running on Unknown Terrain," in *International Conference on Intelligent Robots and Systems*, 2013.
- [5] T. Capehart and C. Moore, "Variable Stiffness Mechanisms Using Spherically Continuously Variable Transmissions," in *International Mechanical Engineering Congress and Exposition*, Houston, 2015.
- [6] A. Biewener, "Biochemistry and Molecular Biology," in *Comparative Biochemistry and Physiology*, 1998, pp. 73-87.
- [7] M. Grebenstein, A. Albu-Schaffer, T. Bahls, M. Chalon, O. Eiberger, W. Friedl, R. Gruber, S. Haddadin, U. Hagn, R. Haslinger, H. Hoppner, S. Jorg, M. Nickl, A. Nothhelfer, F. Petit, J. Reill, N. Seitz, T. Wimbock, S. Wolf, T. Wusthoff and G. Hirzinger, "The dlr hand arm system," in *Robotics and Automation (ICRA) IEEE International Conference*, 2011.
- [8] D. Braun, "Actuated Dynamic Walking in a Seven-Link Biped Robot," *IEEE Transactions on Mechatronics*, vol. 17, no. 1, 1 February 2012.
- [9] M. Hirose and K. Ogawa, *Honda humanoid robots development*, 2007.
- [10] Y. Ogura and et al, "Development of a new humanoid robot WABIAN-2," in *IEEE International Conference on Robotics and Automation*, Orlando, 2006.
- [11] M. Raibert, *Legged Robots That Balance*, Cambridge, MA, USA: Massachusetts Institute of Technology, 1986.

- [12] G. Cavagna, F. Saibene and R. Margaria, "Mechanical work in running," *Journal of Applied Physiology*, pp. 249-256, 1964.
- [13] R. Ham, T. Sugar, B. Vanderborght, K. Hollander and D. Lefeber, "Compliant actuator designs," *Robotics Automation Magazine, IEEE*, pp. 81-94, September 2009.
- [14] J. Hurst, J. Chestnutt and A. Rizzi, "An actuator with physically variable stiffness for highly dynamic legged locomotion," in *Robotics and Automation ICRA '04 IEEE International Conference*, 2004.
- [15] K. Galloway, J. Clark and D. Koditschek, "Design of a tunable stiffness composite leg for dynamic locomotion," in *ASME IDETC/CIE*, 2009.
- [16] A. Enoch, A. Sutas, S. Nakaoka and S. Vijayakumar, "BLUE: A bipedal robot with variable stiffness and damping," in *12th IEEE-RAS International Conference on Humanoid Robots*, 2012.
- [17] Hosoda and et al, "Pneumatic- driven jumping robot with anthropomorphic muscular skeleton structure," *Autonomous Robots*, vol. 28, no. 3, pp. 307-316, 2009.
- [18] S. R. Tonietti and A. Bicchi, "Design and Control of a Variable Stiffness Actuator for Safe and Fast Physical Human/ Robot Interaction," in *IEEE International Conference on Robotics and Automation*, 2005.
- [19] Mitrovic and et al, "Exploiting sensorimotor stochasticity for learning control of variable impedance actuators," in *IEEE- RAS International Conference on Humanoid Robots*, 2010.
- [20] Uemura and S. Kawamura, "A new Mechanical structure for adjustable stiffness device with lightweight and small size," in *IEEEIRSI International Conference on Intelligent Robots and Systems*, 2010.
- [21] Van Ham and et al, "MACCEPA, the mechanically adjustable compliance and controllable equilibrium position actuator: Design and implementation in a biped robot," *Robotics and Autonomous Systems*, vol. 55, no. 10, pp. 761-768, 2007.

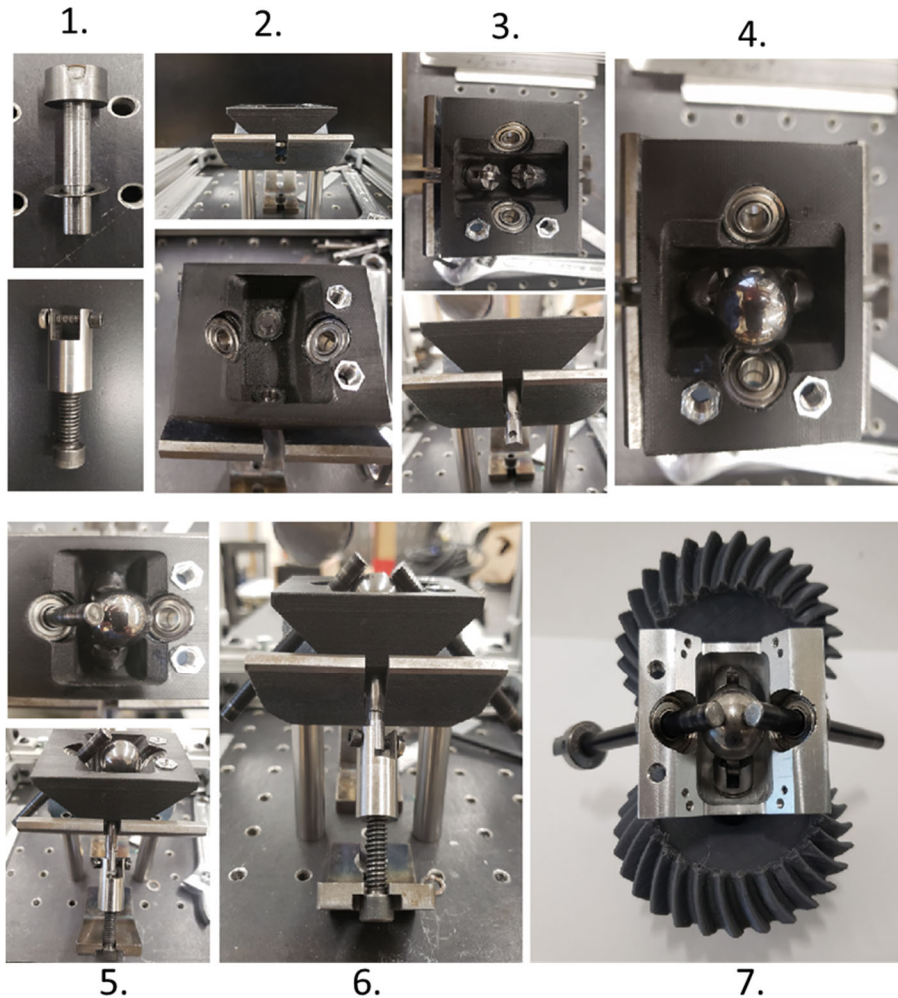
- [22] A. Jafari, N. Tsagarakis and D. Caldwell, "AwAs-ii: A new actuator with adjustable stiffness based on the novel principle of adaptable pivot point and variable lever ratio," in *IEEE International Conference on Robotics and Automation*, 2011.
- [23] T. Morita and S. Sugano, "Development of an anthropomorphic force controlled manipulator WAM-IO," in *International Conference on Advance Robotics*, 1997.
- [24] A. Jafari and et al, "A Novel Actuator with Adjustable Stiffness (AwAS)," in *IEEEIRSJ International Conference on Robotics Automation*, 2010.
- [25] R. J. Full and D. E. Koditschek, "Full, Robert J. and Daniel E. Koditschek. "Templates and anchors: neuromechanical hypotheses of legged locomotion on land," *The Journal of experimental biology*, vol. 202, no. Pt 23, pp. 3325-32, 1999.
- [26] W. Roozing, L. Visser and R. Carloni, "Variable bipedal walking gait with variable leg stiffness," ,, , pp. .," in *5th IEEE RAS/EMBS International Conference on Biomedical Robotics and Biomechatronics*, Sao Paulo, 2014.
- [27] J.-Y. Jun and J. E. Clark, "Jae-Yun Jun, Jonathan E Clark. Characterization of running with compliant curved legs," *Bioinspiration and Biomimetics*, vol. 10, no. 4, 2015.
- [28] L. Visser, S. Stramigioli and R. Carloni, "Control strategy for energy-efficient bipedal walking with variable leg stiffness," in *IEEE International Conference on Robotics and Automation*, Karlsruhe, 2013.
- [29] H. Yu, M. Li, H. Cai and W. Guo, "Stance control of the SLIP hopper with adjustable stiffness of leg spring," in *IEEE International Conference on Mechatronics and Automation*, 2012.
- [30] S. Reise and S. Andre, "Sebastian Riese and Andre Seyfarth. Stance leg control: variation of leg parameters supports stable hopping," *Bioinspiration & biomimetics*, vol. 7, no. 1, 2011.
- [31] M. A. Kluger and D. A. Long, "An Overview of Current Automatic, Manual and Continuously Variable Transmission Efficiencies and Their Projected Future Improvements," *SAE Transactions*, vol. 108, pp. 1-6, 1999.

- [32] M. Peshkin, J. Colgate, W. Wannasuphoprasit, C. Moore, R. Gillespie and P. Akella, "Cobot Architecture," *Robotics and Automation, IEEE Transactions*, pp. 377-390, 2001.
- [33] J. Kim, F. Park and Y. Park, "Desing, Analysis and Control of a Wheeled Mobile Robot with a Nonholonomic Spherical CVT," *Journal of Mechanical Design*, pp. 409-426, 2002.
- [34] K. Tadakuma, R. Tadakuma, K. Terada, A. Ming, M. Shimojo and M. Kaneko, "The Mechanism of the LInear Load-Sensitive Continuously variable transmission with the spherical driving unit," in *Intelligent Robots and System (IROS) IEEE/RSJ International Conference*, 2011.
- [35] K. Songho, C. Moore, M. A. Peshkin and J. Colgate, "Causes of microslip in a continuously variable transmission," *Journal of Mechanical Design*, 2008.
- [36] M. Brokowski, S. Kim, J. Colgate, R. Gillespie and M. Peshkin, Toward improved CVT's: Theoretical and experimental results, 2002.
- [37] X. Zhou and S. Bi, "A survey of bio-Inspired compliant leg designs," *Bioinspiration and Biomemetics*, vol. 7, no. 4, 2012.
- [38] B. Brown and G. Zeglin, "The bow leg hopping robot," in *International Conference on Robotics and Automation*, 1998.
- [39] F. Danion, E. Varraine, M. Bonnard and J. Pailhous, "Stride variability in human giat: the effect of stride frequency and stride length," *Gait and Posture*, vol. 18, no. 1, pp. 69-77, 2003.
- [40] J. Rummel and A. Seyfarth, "Stable Running with Segmented Legs," *International Journal of Robotics Research*, vol. 27, pp. 919-934, 2008.
- [41] D. Ferris, M. Louie and C. Farley, "Running in the real world: adjusting leg stiffness for different surfaces," in *Proceedings. Bioiloical sciences*, 1998.
- [42] B. Miller, J. Schmitt and J. Clark, "Quantifying disturbance rejection of SLIP-like running systems," *Internation Journal of Robotics Research*, pp. 573-587, 2012.

- [44] N. Naclerio et. al., "Low Cost, Continuously Variable, Strain Wave Transmission Using Gecko-Inspired Adhesives," *IEEE Robotics and Automation Letters*, vol. 4, no. 2, pp. 894-901, 2019.
- [45] M. Grenier and C. Gosselin, "Kinematic Optimization of a Robotic Joint with Continuously Variable Transmission Ratio," 2011. [Online]. Available: 6.10.1115/DETC2011-48443.
- [46] E. Mobedi and M. Dede, "Geometrical analysis of a continuously variable transmission system designed for human-robot interfaces.," *Mechanism and Machine Theory*, 2019.

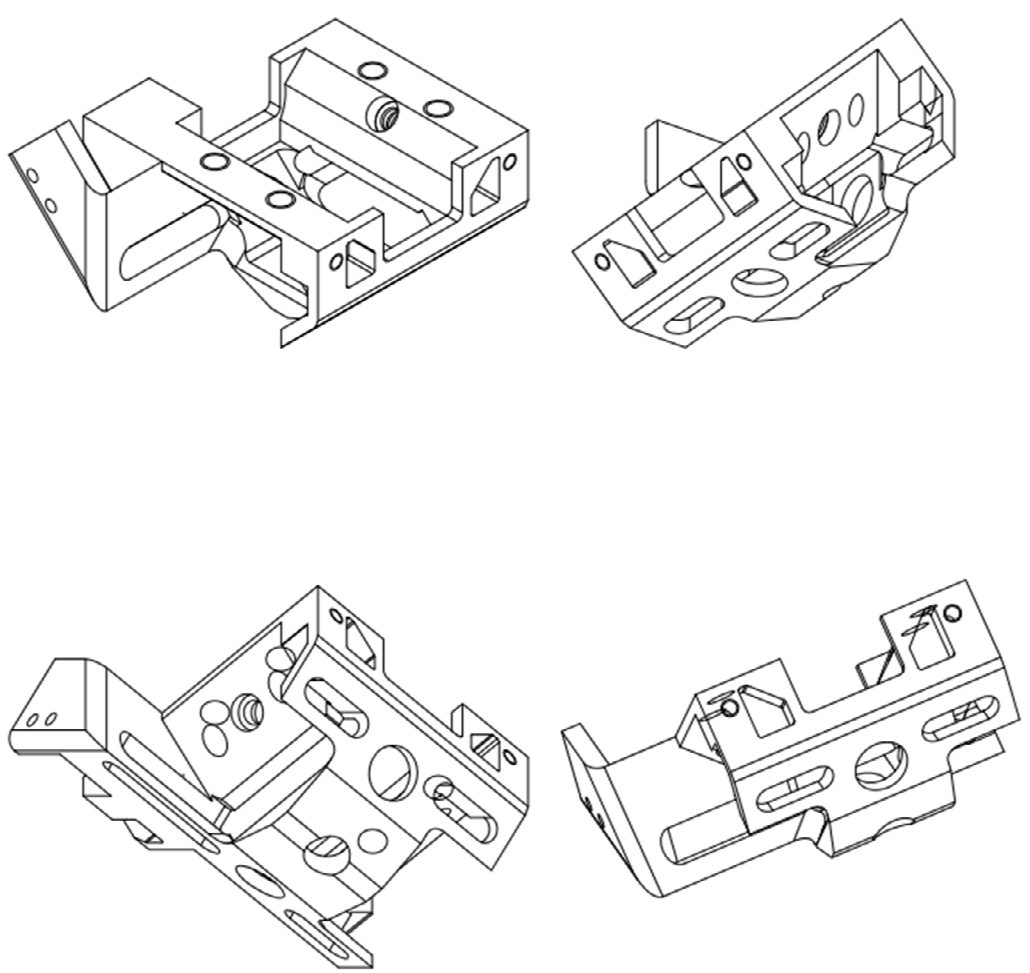
APPENDICES

Appendix A: VSCVT Assembly Process:

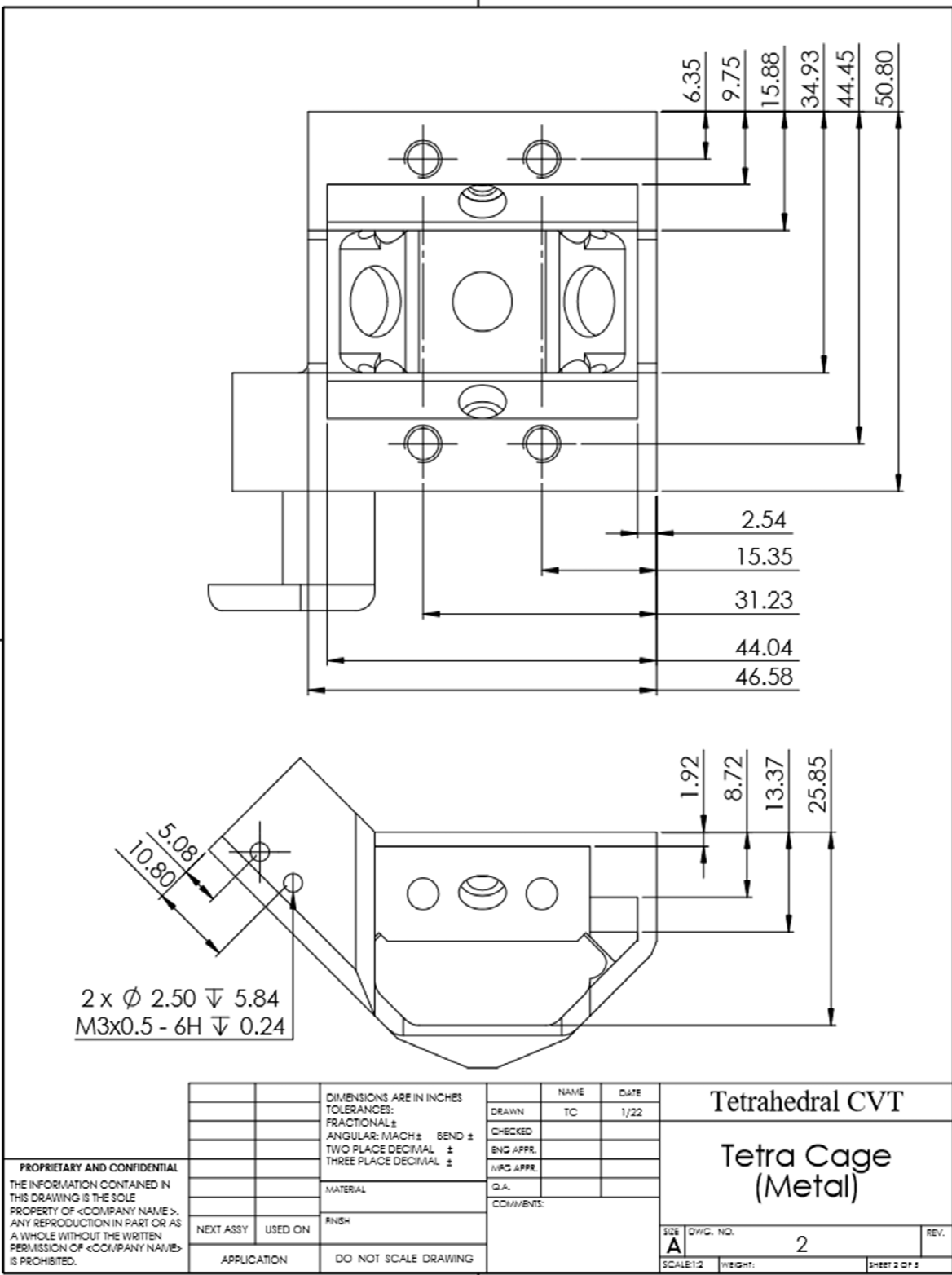


1. Pre-assemble the steering roller shafts and the 1/4 -200 bolt/ nut set
2. Set the CVT support in the preload platform, steering roller shafts aligned with the slots in the plates of the preload stand
3. Insert the steering roller shafts into the steering roller bearings, passing through the slots
4. Place the transmission sphere on top of the steering rollers
5. Couple the bolt/nut set to the steering roller shafts and using the table mounts tighten the screws to compress the springs. Insert drive roller 1.
6. Insert drive roller 2 into its bearing. Loosen the bolts to apply the preload force and aligning the components
7. Remove the bolt/nut set and add the gears to the steering roller shafts. Secure the gears to the steering roller shafts with set screws.

Appendix B: CAD Drawings of CVT Custom Support



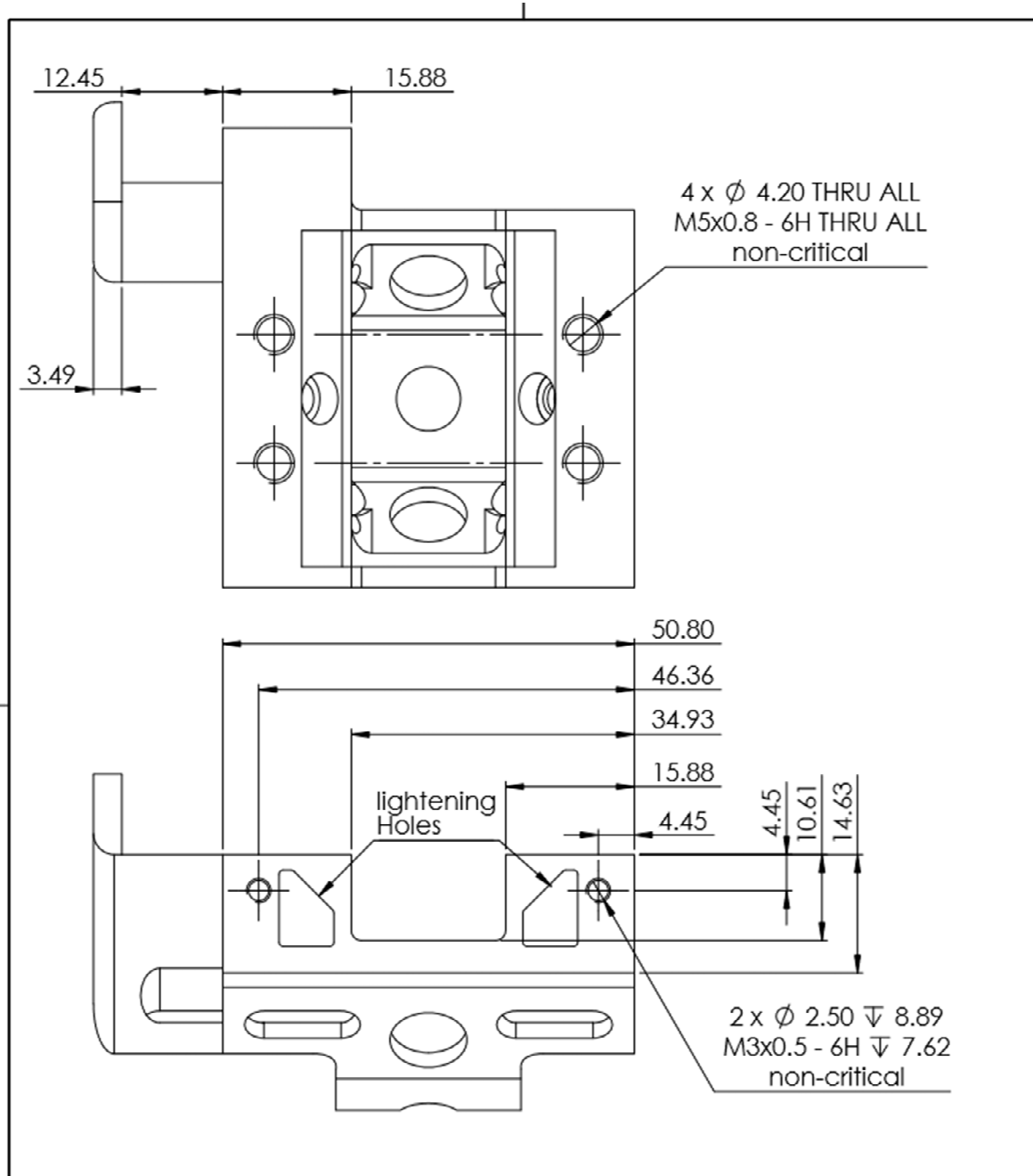
<p>PROPRIETARY AND CONFIDENTIAL THE INFORMATION CONTAINED IN THIS DRAWING IS THE SOLE PROPERTY OF <COMPANY NAME>. ANY REPRODUCTION IN PART OR AS A WHOLE WITHOUT THE WRITTEN PERMISSION OF <COMPANY NAME> IS PROHIBITED.</p>			DIMENSIONS ARE IN INCHES TOLERANCES: FRACTIONAL ± ANGULAR: MACH ± BEND ± TWO PLACE DECIMAL ± THREE PLACE DECIMAL ±		NAME	DATE	Tetrahedral CVT Tetra Cage (Metal)	
					DRAWN	TC		1/22
					CHECKED			
					ENG APPR.			
					MFG APPR.			
				Q.A.				
				COMMENTS:				
			MATERIAL					
			FINISH					
	NEXT ASSY	USED ON						
	APPLICATION		DO NOT SCALE DRAWING					
				SIZE	DWG. NO.	REV.		
				A	2			
				SCALE:1:2	WEIGHT:	SHEET 1 OF 2		



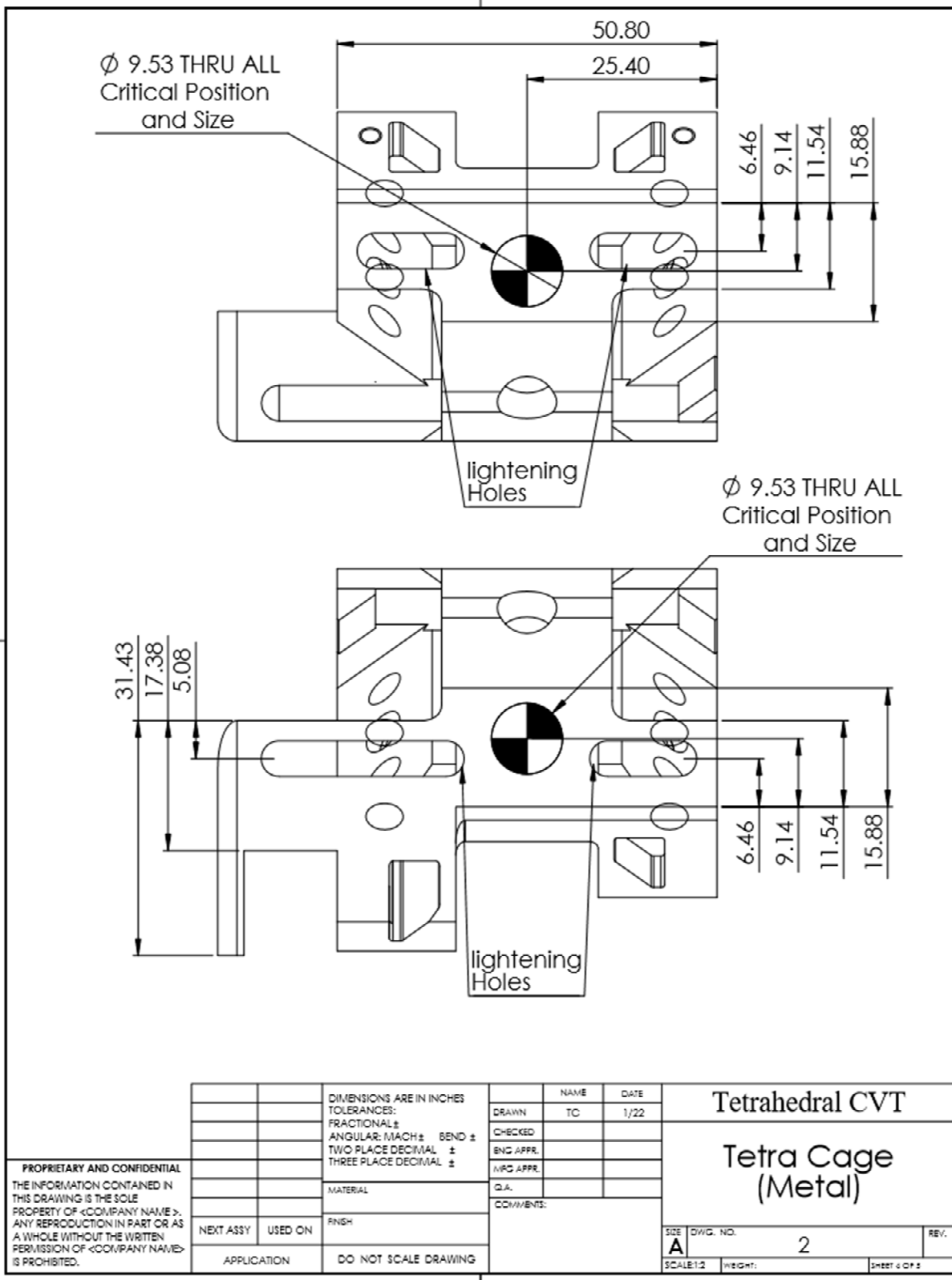
PROPRIETARY AND CONFIDENTIAL
 THE INFORMATION CONTAINED IN THIS DRAWING IS THE SOLE PROPERTY OF <COMPANY NAME>. ANY REPRODUCTION IN PART OR AS A WHOLE WITHOUT THE WRITTEN PERMISSION OF <COMPANY NAME> IS PROHIBITED.

		DIMENSIONS ARE IN INCHES		NAME	DATE
		TOLERANCES:		TC	1/22
		FRACTIONAL ±		CHECKED	
		ANGULAR: MACH ± BEND ±		ENG APPR.	
		TWO PLACE DECIMAL ±		MFG APPR.	
		THREE PLACE DECIMAL ±		Q.A.	
		MATERIAL		COMMENTS:	
NEXT ASSY	USED ON	FINISH			
APPLICATION		DO NOT SCALE DRAWING			

Tetrahedral CVT		
Tetra Cage (Metal)		
SIZE	DWG. NO.	REV.
A	2	
SCALE: 1:2	WEIGHT:	SHEET 2 OF 3



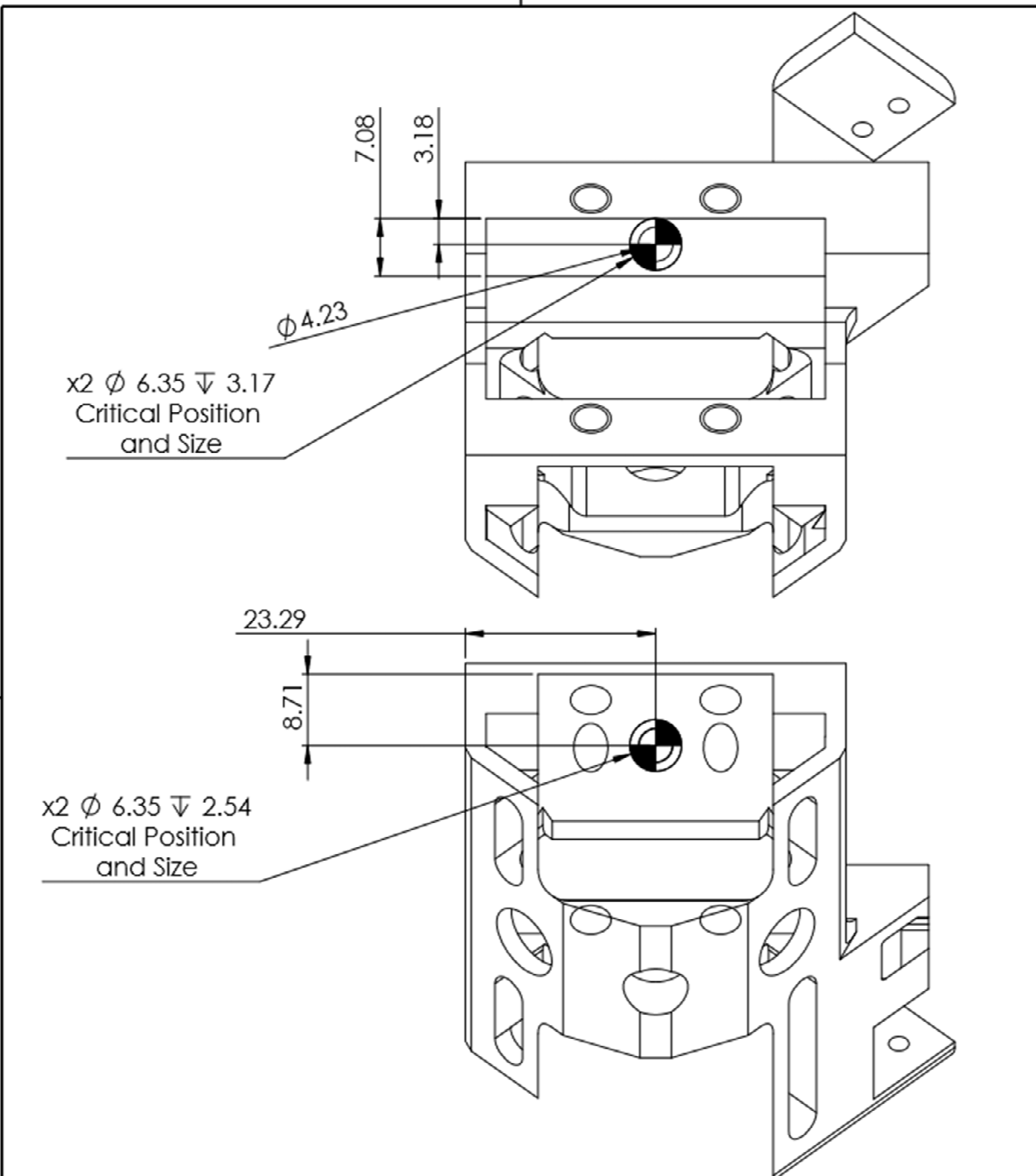
<p>PROPRIETARY AND CONFIDENTIAL THE INFORMATION CONTAINED IN THIS DRAWING IS THE SOLE PROPERTY OF <COMPANY NAME>. ANY REPRODUCTION IN PART OR AS A WHOLE WITHOUT THE WRITTEN PERMISSION OF <COMPANY NAME> IS PROHIBITED.</p>		DIMENSIONS ARE IN INCHES TOLERANCES: FRACTIONAL ± ANGULAR: MACH ± BEND ± TWO PLACE DECIMAL ± THREE PLACE DECIMAL ±		NAME DRAWN TC CHECKED ENG APPR. MFG APPR. Q.A. COMMENTS:	DATE 1/22	Tetrahedral CVT	
		MATERIAL FINISH DO NOT SCALE DRAWING	NEXT ASSY USED ON APPLICATION	SIDE DWG. NO. 2 SCALE: 1:2 WEIGHT: SHEET 3 OF 3		REV.	



PROPRIETARY AND CONFIDENTIAL
 THE INFORMATION CONTAINED IN THIS DRAWING IS THE SOLE PROPERTY OF <COMPANY NAME>. ANY REPRODUCTION IN PART OR AS A WHOLE WITHOUT THE WRITTEN PERMISSION OF <COMPANY NAME> IS PROHIBITED.

		DIMENSIONS ARE IN INCHES		NAME	DATE
		TOLERANCES:		DRAWN	TC
		FRACTIONAL: ±		CHECKED	
		ANGULAR: MACH ± BEND ±		ENG APPR.	
		TWO PLACE DECIMAL ±		MFG APPR.	
		THREE PLACE DECIMAL ±		Q.A.	
		MATERIAL		COMMENTS:	
		FINISH			
NEXT ASSY	USED ON				
APPLICATION		DO NOT SCALE DRAWING			

Tetrahedral CVT		
Tetra Cage (Metal)		
SIZE	DWG. NO.	REV.
A	2	
SCALE: 1:2	WEIGHT:	SHEET 4 OF 5



PROPRIETARY AND CONFIDENTIAL THE INFORMATION CONTAINED IN THIS DRAWING IS THE SOLE PROPERTY OF <COMPANY NAME>. ANY REPRODUCTION IN PART OR AS A WHOLE WITHOUT THE WRITTEN PERMISSION OF <COMPANY NAME> IS PROHIBITED.		DIMENSIONS ARE IN INCHES		NAME	DATE	Tetrahedral CVT Tetra Cage (Metal)	
		TOLERANCES:		DRAWN	TC		1/22
		FRACTIONAL: \pm		CHECKED			
		ANGULAR: MACH \pm BEND \pm		ENG APPR.			
		TWO PLACE DECIMAL \pm		MFG APPR.			
		THREE PLACE DECIMAL \pm		Q.A.			
		MATERIAL		COMMENTS:			
NEXT ASSY	USED ON	FINISH					
APPLICATION		DO NOT SCALE DRAWING					
				SIZE	DWG. NO.	REV.	
				A	2		
				SCALE: 1:2	WEIGHT:	SHEET 2 OF 2	

Appendix C: Teensy 3.2 Control and Data Acquisition Program

```
// Header Files

#include <SPI.h>    // Enables SPI communication needed for communicating with SD
Card
#include <SD.h>    // Enables SD Card read and write functions
#include <Servo.h>  // Enables Servo Objects
#include <Wire.h>   // Enables I2C Communication need for communicating with
IMU
#include <math.h>
#define ENCODER_OPTIMIZE_INTERRUPTS
#include <Encoder.h> // Enables interrupt-based encoder reading on all digital pins

// The circuit:
// * SD card attached to SPI bus as follows:

// SPI Pins Initialization
#define CHIP_SEL    10
#define MOSI_PIN    11
#define MISO_PIN    12
#define CLK_PIN     13

////////// DEFINE PIN LOCATIONS //////////
// Encoder Reset and TD Sensor
#define RESET_SWTCH 3
#define FT_SWTCH    5
#define SWTCH_PWR1  4 //pwr for foot switch`
#define SWTCH_PWR2  6 //pwr for reset switch

// Encoder Initializations
//Definitions for Encoder 1: Boom encoder
#define ENC_1_1     14
#define ENC_1_2     15

// Definitions for Encoder 2: Slider crank motor encoder
#define ENC_2_1     16
#define ENC_2_2     17

//Definitions for Encoder 3: CVT input encoder
#define ENC_3_1     18
#define ENC_3_2     19

//Definitions for Encoder 4: CVT output encoder
#define ENC_4_1     20
#define ENC_4_2     21
```



```

//PWM pins for motor driver
//Motor Driver Switch to md07a
#define Dir 23
#define PWMpin1 22

//////// DEFINE CONSTANTS //////////
#define kP      10
#define kD      1
#define TICKS_PER_REV1 3978 // 64 CPR * 16.5765(:1) Gearbox * 3.75(:1)
ExternalGear Rounded to nearest int
#define PWM_MAX 255
#define PWM_MIN 0
#define INIT_FREQ 1
#define CONTROL_TIME 1000 // microSec 1000
#define SENSOR_TIME 10000 // microSec 10000
#define LOG_TIME 10000
#define INTERVAL 100 // milliSec 100
//define SERVO_CENTER 101 // deg

//////// Flags for Debugging //////////
#define DISP 1
#define TEST 0
#define LOG 1
#define SEC_ENC 1

#define fileName "FT_TIM1.txt"

//////// Initialization of Objects //////////
// Set up Encoder object for both motors
Encoder ENC1(ENC_1_1, ENC_1_2);
#if (SEC_ENC)
Encoder ENC2(ENC_2_1, ENC_2_2);
Encoder ENC3(ENC_3_1, ENC_3_2);
Encoder ENC4(ENC_4_1, ENC_4_2);

#endif

#include <PWMServo.h>
PWMServo myservo;
// Set up Real time interrupts (Believe this does multithreading)
IntervalTimer Control;
IntervalTimer Update;
IntervalTimer Sensor;

```

```

///// Define Global Variables /////
// Control Variables
volatile long des_ang2 = 180;
volatile long cur_pos1;
volatile long prev_pos1 = 0;
volatile long des_pos1 = 0;
volatile double des_pos1f = 0;
volatile double prev_des1 = 0;
volatile long cur_pos2;
volatile long prev_pos2 = 0;
volatile long des_pos2 = 0;
volatile double des_pos2f = 0;
volatile double prev_des2 = 0;
volatile float trns_ratio = 0;
volatile long cur_pos3;
volatile long prev_pos3 = 0;
volatile long des_pos3 = 0;
volatile double des_pos3f = 0;
volatile double prev_des3 = 0;
volatile long cur_pos4;
volatile long prev_pos4 = 0;
volatile long des_pos4 = 0;
volatile double des_pos4f = 0;
volatile double prev_des4 = 0;
volatile long err2a;

volatile float cur_ang1;
volatile float prev_ang1;
volatile float cur_ang2;
volatile float prev_ang2;
volatile float cur_ang3;
volatile float prev_ang3;
volatile float cur_ang4;
volatile float prev_ang4;

volatile long ft_swch;
volatile long reset_swch;
volatile int pwm_val1;

// Calculated variables used in multiple functions
volatile float des_TRANS = 0; //Hz
volatile float act_des_TRANS = 0; //Hz
volatile float VEL1 = 0; // Hip velocity (check units)
volatile float VEL2 = 0; // Motor Velocity ( convert to deg/sec)
volatile float VEL3 = 0; //CVT input velocity

```

```

volatile float  VEL4      = 0; //CVT output velocity

volatile float  VEL1L     = 0; // deg
volatile float  VEL2L     = 0;
volatile float  VEL3L     = 0;
volatile float  VEL4L     = 0;
volatile float  Hop_height;
// Spring distance value
volatile int  dist_sens;

// Time variables
volatile long  curr_time;
volatile long  prev_time;
volatile long  prev_time3;
volatile long  tail_start;
volatile long  start = 0;

// Data Logging Variables
volatile long  data_val[20];
volatile int   data_length = 0;
int  pos = 0;
// Tail Servo Control Variables
//volatile int  serv_pos;
//volatile int  max_ang = 0;
//volatile int  ang;

volatile int  SD_FLAG = 0;

String tmpArr = "";
volatile float runVal[3] = {0};
//volatile int  num;

int  prev_time2 = 0;

void setup() {
  char test;
  int  numBytes = 0;
  // put your setup code here, to run once:
  pinMode(LED_BUILTIN, OUTPUT);
  Serial.begin(9600);
  Serial.println("Serial Initialization Complete");

  ENC1.write(0);
  ENC2.write(0);
  ENC3.write(0);

```

```

ENC4.write(0);

start = millis();

//set pin modes
pinMode(PWMPin1,OUTPUT);
pinMode(Dir,OUTPUT);
pinMode(RESET_SWTCH,INPUT);
pinMode(FT_SWTCH,INPUT);
pinMode(SWTCH_PWR1,OUTPUT);
pinMode(SWTCH_PWR2,OUTPUT);

analogWrite(SWTCH_PWR1,255);
analogWrite(SWTCH_PWR2,255);

//Set up Interrupts for Control and Sensor Readings
// Control.begin(PD_Control, 1000); // blinkLED to run every 0.001 seconds
Update.begin(GetStatus, CONTROL_TIME); // blinkLED to run every 0.001 seconds
Sensor.begin(GetSensor, SENSOR_TIME); // blinkLED to run every 0.0001 seconds

Serial.print("Initializing SD card...");

// see if the card is present and can be initialized:
if (!SD.begin(CHIP_SEL)) {
  Serial.println("Card failed, or not present");
  SD_FLAG = 1;
}
Serial.println("card initialized.");

File runFile = SD.open("CVT_RUN.txt");

if(runFile)
{
  int j = 0;
  int k = 0;
  numBytes = runFile.available();
  for(int i = 0; i < numBytes; i++)
  {
    test = runFile.read();
    if(test != ',')
    {
      tmpArr += test;
    }
    else
    {

```

```

        runVal[k] = tmpArr.toFloat();
        tmpArr = "";
        k++;
    }
}
runFile.close();
}
else
{
    act_des_TRANS = 0.0;
}

if(LOG)
{
    String introString = "";

    // introString = "CVT Run ENC VEL = " + String(act_des_TRANS) + " VEL 1 = " +
String(VEL1) + " VEL 2 = " + String(VEL2);
    introString = "Test 1 - Hop height 30V _ State Controller_NO PD_data log" ;

    File dataFile = SD.open(fileName, FILE_WRITE);

    if (dataFile) {
        dataFile.println("-----");
        dataFile.println(introString);
        dataFile.println("-----");

        dataFile.println("");
        dataFile.println("");
        dataFile.close();
        // print to the serial port too:
        Serial.println(introString);
    }
}

// Get Current Encoder Values and Compute Current Error in Pos and Vel
// Then Compute the PWM Value for each motor
void GetStatus(void)
{
    long err;
    long err2;
    long err2a;

    curr_time = (millis() - start);

```

```

prev_ang1 = (double)prev_pos1/(2048*4)*(360); //convert encoder counts to angle in
degrees - 2048 counts per rev quad
prev_ang2 = (double)prev_pos2/(7064*4)*(360); //gear ratio 676/49 - 512 counts per
rev quad
prev_ang3 = (double)prev_pos3/(2048*4)*(360);
prev_ang4 = (double)prev_pos3/(2048*4)*(360);

cur_pos1 = ENC1.read();
cur_pos2 = ENC2.read();
cur_pos3 = ENC3.read();
cur_pos4 = ENC4.read();

ft_swth = digitalRead(FT_SWTCH);
reset_swth = digitalRead(RESET_SWTCH);

}

void GetSensor(void)
{
long err;
long err2;
long err3;
float boom_length = 116; //length of foot to pivot boom (cm)

cur_ang1 = (float)cur_pos1/(2048*4)*(360); //Hip angle
cur_ang2 = (float)cur_pos2/(7064*4)*(360); //Slider Crank motor angle
cur_ang3 = (float)cur_pos3/(2048*4)*(360); //CVT input angle
cur_ang4 = (float)cur_pos4/(2048*4)*(360); //CVT output angle

err = des_pos1 - cur_pos1;
VEL1 = (cur_ang1 - prev_ang1)/(0.01);
err2 = des_pos2 - cur_pos2; //slider crank angle error
VEL2 = (cur_ang2 - prev_ang2)/(0.01); //slider crank velocity
err3 = des_pos3 - cur_pos3;
VEL3 = (cur_ang3 - prev_ang3)/(0.01);

err2 = des_ang2 - cur_ang2; //slider crank angle error

VEL1L = (cur_ang1 - prev_ang1)/(0.000001);
VEL2L = (cur_ang2 - prev_ang2)/(0.000001);
VEL3L = (cur_ang3 - prev_ang3)/(0.000001);

prev_pos1 = cur_pos1;
prev_des1 = des_pos1f;
prev_pos2 = cur_pos2;

```

```

prev_des2 = des_pos2f;
prev_pos3 = cur_pos3;

trns_ratio = VEL4/VEL3;

Hop_height = boom_length*(cur_ang1*PI/180);

if(LOG)
{
  data_val[0] = curr_time;
  data_val[1] = cur_pos1; //Hip encoder counts raw
  data_val[2] = cur_ang1; //Hip encoder angle
  data_val[3] = prev_pos1; //Previous value for velocity calculation
  data_val[4] = VEL1L; //velocity of hip
  data_val[5] = cur_pos2; //SC motor encoder counts raw
  data_val[6] = cur_ang2; //SC motor angle
  data_val[7] = prev_pos2; //Previous value for velocity calculation
  data_val[8] = VEL2L; //Velocity of slider crank
  data_val[9] = ft_swch; //TD indicator
  data_val[10] = reset_swch;
  data_val[11] = Hop_height;

  data_length = 12;
}
}

void loop() {
  int value = 10;
  if((DISP) && (curr_time - prev_time2) > INTERVAL)
  {
    Serial.print("Slider Crank Angle = ");
    Serial.print(cur_ang2);
    Serial.print("\tfoot Switch State = ");
    Serial.print(ft_swch);
    Serial.print("\tLeg hop height = ");
    Serial.print(Hop_height);
    Serial.print("\tPWM Value = ");
    Serial.println(pwm_val1);

    if(SD_FLAG)
      Serial.println("SD CARD FAILED");
    else
    {
      Serial.print("Slider Crank Angle = ");
      Serial.print(cur_ang2);
    }
  }
}

```

```

    Serial.print("\tFoot Switch State = ");
    Serial.print(ft_swch);
    Serial.print("\tLeg Hop Height = ");
    Serial.print(Hop_height);
    Serial.print("\tPWM Value = ");
    Serial.println(pwm_val1);
}

if(ft_swch == HIGH){          //Leg is in flight phase
    if(reset_swch == LOW){    //reset swch is pressed
        ENC2.write(0);
        digitalWrite(Dir,HIGH);
        analogWrite(PWMPin1,0);
    }
    else{
        analogWrite(PWMPin1,250);
    }
}

else{                          //Leg is in stance phase
    if(VEL1L<1000000){        //boom has reached full compression and is moving up

pwm_val1 = 255;

        analogWrite(PWMPin1,pwm_val1);
        digitalWrite(Dir,HIGH);

    }
    else{                       //boom is in touch down but has not reached max compression
        digitalWrite(Dir,HIGH);
        analogWrite(PWMPin1,0);
        //Serial.println(value);
    }
}

if(LOG)
{
    String dataString = "";
    // read three sensors and append to the string:
    for (int i = 0; i < data_length; i++) {
        long sensor = data_val[i];
        dataString += String(sensor);
        if (i < data_length) {
            dataString += ",";

```



```
    }  
  }  
  
  File dataFile = SD.open(fileName, FILE_WRITE);  
  
  if (dataFile) {  
    dataFile.println(dataString);  
    dataFile.close();  
    // print to the serial port too:  
  //   Serial.println(dataString);  
    }  
  // if the file isn't open, pop up an error:  
  else {  
  //   Serial.println("error opening datalog.txt");  
    }  
  }  
}
```